iScience

CellPress
OPEN ACCESS

Article

An enhanced machine learning-based prognostic prediction model for patients with AECOPD on invasive mechanical ventilation

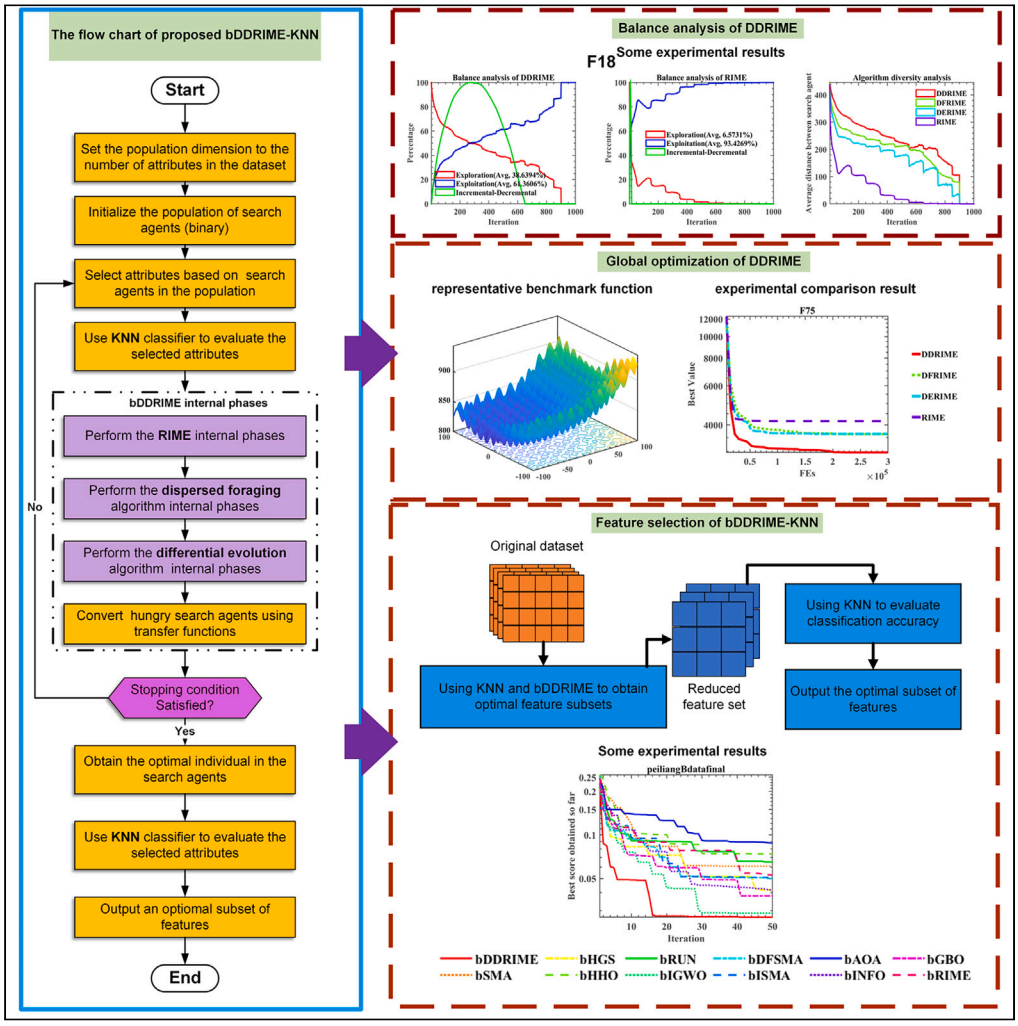

Yujie Fu, Yining Liu, Chuyue Zhong, ..., Sudan Yu, Huiling Chen, Peiliang Wu

yusudan07@sina.com (S.Y.)
chenhuiling.jlu@gmail.com (H.C.)
pl_wu@163.com (P.W.)

Highlights

We propose an improved RIME with dispersed foraging and differential crossover

The balance, diversity, and function tests show the effect of DDRIME

The DDRIME-KNN outperforms other methods on datasets for feature selection

This model performs well for patients with AECOPD on invasive mechanical ventilation

Fu et al., iScience 27, 111230
December 20, 2024
https://doi.org/10.1016/j.isci.2024.111230

iScience

CellPress
OPEN ACCESS

Article

An enhanced machine learning-based prognostic prediction model for patients with AECOPD on invasive mechanical ventilation

Yujie Fu,[1,7] Yining Liu,[1,7] Chuyue Zhong,[2] Ali Asghar Heidari,[3] Lei Liu,[4] Sudan Yu,[5,*] Huiling Chen,[6,8,*] and Peiliang Wu[1,*]

SUMMARY

Chronic obstructive pulmonary disease (COPD) causes irreversible airflow limitations, increasing global morbidity and mortality. Acute exacerbations (AECOPDs) worsen symptoms and may require mechanical ventilation, leading to complications. Understanding factors affecting AECOPD prognosis during mechanical ventilation is crucial. Inspired by rime ice physics, the RIME algorithm has been proposed but it had limitations in feature selection and solution space exploration. We improve RIME by adding a dispersed foraging mechanism and differential crossover operator, creating DDRIME. Our study analyzes patient data to identify factors related to invasive mechanical ventilation in AECOPD. DDRIME's performance is tested against RIME on 83 functions and 12 public datasets for feature selection. It outperformed most algorithms, with bDDRIME_KNN showing high accuracy in predicting AECOPD outcomes. Key indicators—chronic heart failure (CHF), D-dimer (D-D), fungal infection (FI), and pectoral muscle area (PMA)—predicted prognosis with >0.98 accuracy. bDDRIME is thus a valuable tool for predicting AECOPD patients' outcomes on mechanical ventilation.

INTRODUCTION

Chronic obstructive pulmonary disease (COPD) is a pervasive respiratory condition, often attributed to long-term exposure to harmful substances such as tobacco smoke, air pollutants, and occupational dust. This exposure initiates a cascade of inflammatory responses, leading to the progressive deterioration of lung function.[1] Common symptoms of COPD include persistent cough, excessive sputum production, and shortness of breath, especially during physical activities. As the disease progresses, patients may experience exacerbations that significantly impact their quality of life.[2] Patients are more susceptible to exacerbations, which can severely diminish their quality of life. The global impact of COPD is substantial, with recent data from the World Health Organization indicating it as the third leading cause of death worldwide, accounting for over 3 million deaths annually. It is noteworthy that a disproportionate burden of these fatalities occurs in low- and middle-income countries, underscoring an urgent need for effective public health strategies.[3,4] With an aging population and smoking as a major cause, COPD has a high global prevalence, while nearly 90% of mortality is seen in low- and middle-income countries, and its mortality rate is in the top three of age-standardized mortality rates for both sexes.[5]

Acute exacerbation of chronic obstructive pulmonary disease (AECOPD) is an event of exacerbation of respiratory symptoms due to a short-term increase in inflammatory cells in the blood for 7–10 days or more caused by viral or bacterial infection of the respiratory tract.[3] Inpatient AECOPD usually has rapid changes in disease, reduced oxygen saturation, and the presence of severe other comorbidities. In addition to basic medication and oxygen therapy, the preferred mode of ventilation in combined respiratory failure is noninvasive ventilation (NIV),[6] but the failure rate is still 5%–40%,[7] and when NIV fails, it should be changed to invasive mechanical ventilation (IMV) as a follow-up treatment. However, the use of IMV after NIV failure increases the duration of ventilation while increasing complications related to mechanical ventilation such as respiratory-associated pneumonia and in-hospital mortality.[8] Therefore, early identification of the causes of IMV failure and prolonged ventilation time can lead to the adjustment of an accurate treatment plan for patients, thus improving prognosis, reducing the length of hospital stay, and decreasing mortality.

[1]Department of Pulmonary and Critical Care Medicine, The First Affiliated Hospital of Wenzhou Medical University, Wenzhou 325000, China
[2]The First Clinical College, Wenzhou Medical University, Wenzhou 325000, China
[3]School of Surveying and Geospatial Engineering, College of Engineering, University of Tehran, Tehran, Iran
[4]College of Computer Science, Sichuan University, Chengdu, Sichuan 610065, China
[5]Department of Artificial Intelligence, Wenzhou Polytechnic, Wenzhou 325035, China
[6]Department of Computer Science and Artificial Intelligence, Wenzhou University, Wenzhou 325035, China
[7]These authors contributed equally
[8]Lead contact
*Correspondence: yusudan07@sina.com (S.Y.), chenhuiling.jlu@gmail.com (H.C.), pl_wu@163.com (P.W.)
https://doi.org/10.1016/j.isci.2024.111230

Machine learning is an emerging field of study that focuses on the development of algorithms and statistical models for computers to perform tasks. without explicit programming. It is increasingly being applied in the field of respiratory diseases, especially in the early diagnosis,[9] disease change prediction, and prognosis of lung cancer,[10] COPD,[11] interstitial lung diseases,[12] and seizure prediction.[13] As machine learning has advanced, its applications have spread across various industries, especially in the medical field, becoming a powerful assistant for radiologists and clinicians. In medical-related research,[14] widely-used algorithms encompass support vector machines (SVMs), decision trees, neural networks,[15,16] deep learning,[1] and so on.[17] It provides great value. This not only allows to reduce the burden of imaging physicians but also provides a reference for clinicians' treatment decisions, thus reducing unnecessary costs for patients at a later stage and improving disease prognosis and survival rates.[18]

Conventional optimization methods, like exhaustive enumeration and Newton's method, often get stuck in local optima and result in high computational complexity for these problems. In contrast, metaheuristic algorithms (MAs) have attracted considerable attention because of their flexibility, simplicity, and ability to avoid local optima.[19,20] It has been widely applied in economic emission,[21,22] medical diagnosis,[23,24] and parameter optimization.[25] Moreover, due to its strong ability to escape local optima, it shows great promise in fields such as image dehazing,[26,27] text privacy,[28] vehicle communication,[29] and video deblurring.[30]

Recently, MAs have advanced significantly and have been widely applied to feature selection. There are several algorithms reported, such as genetic algorithm (GA),[31] hunger games search (HGS),[32] artemisinin optimization,[33] polar lights optimization,[34] differential evolution (DE),[35] slime mold algorithm (SMA),[36] fata morgana algorithm,[37] colony predation algorithm,[38] the weighted mean of vectors (INFO),[39] educational competition optimizer,[40] parrot optimizer,[41] Runge Kutta optimizer (RUN),[42] Harris hawks optimization (HHO),[43] liver cancer algorithm,[44] and so on. Chen et al. put forward HGS-based k-nearest neighbor (KNN) for high-dimensional feature selection.[45] Wu et al. introduced an evolving fuzzy k-nearest neighbor (FKNN) approach, enhanced by a sine cosine algorithm, for diagnosing lupus nephritis. This method offers a viable solution for clinical decision-making.[46] Wang et al. used an enhanced moth flame optimization with SVMs to assist in lupus nephritis diagnosis.[47] Hu et al. developed the potential of a kernel extreme learning machine (KELM) model using an enhanced binary HHO for the early accurate evolution of COVID-19 severity.[48] Ye et al. presented a multilayer perceptron (MLP)-based ant lion optimization method to find a proper solution through the predictive intelligence process.[49] Therefore, there are many classifiers based on MAs, including KNN, FKNN, SVM, KELM, MLP, and so on.

Su et al. introduced an MA called RIME in 2023, drawing inspiration from the phenomenon of rime ice.[50] While RIME has yielded promising results in various engineering applications and on benchmark datasets, it struggles with feature selection due to limited exploration space, leading to local optima entrapment and unsatisfactory convergence. To enhance RIME's accuracy and avoid local optima, we introduce an enhanced version named DDRIME that combines dispersed foraging with a differential crossover operator. On one hand, the dispersed foraging mechanism forces a portion of individuals to be dispersed into a new region to forage. This dispersal behavior makes it possible to find an area with abundant food. On the other hand, the differential crossover operator further boosts the algorithm's exploration capacity, helping to avoid entrapment in local optima and enhance individual optimization capabilities within the algorithm. To evaluate its performance, we evaluate DDRIME against some existing algorithms on 83 functions. Our analysis, employing the Wilcoxon signed-rank test (WSRT)[51] and the Friedman test (FT),[52] reveals that DDRIME outperforms both the conventional RIME algorithm and other MAs. Additionally, to address the computational challenges and suboptimal performance of conventional feature selection methods, we employ statistical measures such as average (AVG), standard deviation (SD), and WSRT in the experiment. These metrics validate the optimization performance of the DDRIME method.

In summary, the primary contributions of this work are as follows.

(1) We proposed the RIME algorithm based on the dispersed foraging mechanism and differential crossover operator to improve the global exploration search capacity and the likelihood of discovering the optimal solution.
(2) Through comparisons with several well-known algorithms on function tests, we have confirmed the exceptional performance of DDRIME. Furthermore, we have applied the binary version of DDRIME based on KNN for feature selection.
(3) Experimental comparisons show that the DDRIME-KNN model outperforms many other methods on the public datasets for feature selection, and the findings demonstrate that this method can improve accuracy.
(4) The DDRIME-KNN model compares against other classifiers and other algorithms on patients with AECOPD undergoing IMV dataset.

This single-center case-control study retrospectively collected medical records related to patients with AECOPD who underwent tracheal intubation at hospital from October 2016 to October 2021 at the First Affiliated Hospital of Wenzhou Medical University, which is the AECOPD dataset. The Clinical Research Ethics Committee of the First Affiliated Hospital of Wenzhou Medical University approved and reviewed this study with the ethical approval code KY2023-R054.

Combined with the Global Initiative for Chronic Obstructive Lung Disease 2013, those who met the following 3 criteria were included: (1) the diagnostic criteria for COPD (forced expiratory volume in 1 s (FEV1)/forced vital capacity (FVC) <0.70 after inhalation of bronchodilators) were met by spirometry, the current cough, sputum, and dyspnea were worse than usual, or the amount of sputum was increased, or yellow sputum was coughed up, and a change in the medication regimen was required; (2) invasive ventilator-assisted ventilation was used during treatment; and (3) tracheal intubation was performed in our hospital. Those who had any of the following were excluded: (1) abandoned treatment for financial reasons, (2) tracheal intubation performed in an outside hospital, and (3) incomplete clinical data. IMV was defined to be failed based on the following: (1) in-hospital death of a patient on IMV, (2) automatic discharge in critical condition, and (3) difficulty in withdrawing the machine from the patient.

Table 1. General characteristics of this study and its abbreviations

	Features	Abbreviation
C1	fungal infection	FI
C2	multidrug resistant bacteria infection	MDROI
C3	chronic heart failure	CHF
C4	age	Age
C5	gender	Gender
C6	smoking history	SH
C7	pectoral muscle area	PMA
C8	D-dimer	D-D
C9	fibrinogen	FIB
C10	cardiopulmonary resuscitation	CPR
C11	brain natriuretic peptide	BNP
C12	bilirubin	BR
C13	total protein	TP
C14	albumin	ALB
C15	serum creatinine	SCR
C16	total cholesterol	TC
C17	coronary artery disease	CAD
C18	cerebral vascular disease	CVD
C19	diabetes mellitus	DM
C20	chronic renal failure	CRF

The 84 patients were divided into the group with successful IMV ($n = 46$) and the group with failed IMV ($n = 38$) according to the prognosis of IMV. All patients' general information, blood test results, and other disease comorbidities are recorded. This study was statistically analyzed using the SPSS 26.0 statistical software. Continuous variables with a normal distribution were analyzed using the Kolmogorov-Smirnov test and presented as mean ± standard deviation (_X ± S), and the u test was utilized for comparison. Continuous variables with nonnormal distribution were analyzed using non-parametric tests and described as the median and interquartile range (IQR), count data were presented as percentages (%), and t comparisons between groups were conducted using the chi-squared test or Fisher's exact test. Table 1 lists all metrics, and their statistical analyses are presented in Tables 2 and 3.

RESULTS AND DISCUSSION

To demonstrate the positive performance of the dispersed foraging strategy and differential crossover operator on RIME, comparative experiments are done on 83 functions. The effect of DDRIME is proved by comparing it to well-known algorithms on function tests. Subsequently, the binary version of DDRIME is used to select features on the public datasets. Lastly, the new algorithm is applied to the dataset to select the optimal subset. The results validate that DDRIME solves the feature selection problem effectively. To reduce the impact of randomness and enhance the reliability of the results, the maximum number of iterations is 300,000 and the population size is 30. Each method is executed independently 30 times. In the experiments, the average value and ranking of the methods on functions are obtained by WRST and the FT, which analyzed statistical results, with the following parameters: an alpha level of 0.05 and an anticipated effect size based on literature review.[53] The calculated minimum sample size required to achieve statistical significance was 0.05, which was then used to guide our recruitment strategy. All tests in this work are performed on a Windows 11 machine utilizing MATLAB R2018b, featuring a 12th Gen Intel(R) Core (TM) i7-12700H (2.30 GHz) CPU and 16.0 GB of RAM.

The interaction of the two mechanisms

There are 83 benchmark functions to evaluate the interaction of dispersed foraging mechanism and differential crossover operator on RIME, including 23 classic function sets and 60 CEC functions. F1–F23 are the classic functions, F24–F53 are the CEC2014 benchmark functions,[54] and F54–F83 are the CEC2017 competition functions.[4] Test functions can be grouped into four categories: unimodal, hybrid, multimodal, and composition. To demonstrate the robustness and applicability of DDRIME effectively, it is compared with the dispersed foraging RIME (DFRIME), the differential evolution RIME (DERIME), and the conventional RIME. To be fair, all methods are conducted in the same experimental environment. Meanwhile, to reduce the impact of randomness and enhance the reliability of the results, the maximum number of iterations is 300,000 and the population size is 30. Each method is executed independently 30 times. In the experiments, the average value and ranking of the methods on functions are obtained by WRST[51] and the FT,[52] which analyzed statistical results.

Table 2. General characteristics and comorbidities of the successful and unsuccessful invasive mechanical ventilation groups

Index		Successful mechanical ventilation group (n = 46)	Mechanical ventilation failure group (n = 38)	χ^2 value	p value
Gender	male	67.40%	76.30%	0.812	0.367
	female	32.60%	23.70%		
SH	no	58.70%	60.50%	0.029	0.865
	yes	41.30%	39.50%		
FI	no	91.30%	52.60%	16.100	0.000
	yes	8.70%	47.40%		
MDROI	no	87.00%	78.90%	0.961	0.327
	yes	13.00%	21.10%		
CHF	no	82.60%	60.50%	5.103	0.024
	yes	17.40%	39.50%		
CAD	no	87.00%	89.50%	0.000	0.987
	yes	13.00%	10.50%		
CVD	no	91.30%	86.80%	0.092	0.761
	yes	8.70%	13.20%		
DM	no	73.90%	76.30%	0.064	0.800
	yes	26.10%	23.70%		
CRF	no	93.50%	92.10%	0.000	1.000
	yes	6.50%	7.90%		

Comparison of mechanisms on benchmark functions

In the proposed method, we employ a dispersed foraging mechanism and differential crossover operator to amplify the population's exploration, thereby improving the optimization performance of RIME. To assess the influence of the mentioned two strategies on RIME, ablation experiments are conducted on 83 benchmark functions. Table 4 shows the algorithms with mechanisms, where "DF" represents the dispersed foraging mechanism and "DE" denotes the differential crossover operator. Table 5 presents the results of different variants on the test set. Figure 1 illustrates convergence curves of RIME's variants on selected functions. Figure 2 presents the balance and diversity analysis of DDRIME, compared to the original RIME.

In Table 5, "AVG" denotes the average results over 30 test function runs, while "SD" is the standard deviation. In Table 6, "AVR" denotes the statistical evaluation of the algorithm's mean performance on 83 benchmark functions. "Rank" indicates the ranking of the algorithm's effectiveness. From Tables 5 and 6 and Figure 1, it is evident that incorporating the dispersed foraging mechanism enhances the algorithm's exploration capability within the search space. Integrating these two strategies with RIME enhances population exploration and local exploitation, preventing agents from becoming trapped in local optima and increasing the chances of finding the global optimum. Comparative experimental evidence supports that the integration of dispersed foraging and differential crossover operators can significantly strengthen RIME.

To further evaluate DDRIME, a set of experiments is used, and their results are discussed. In the balance analysis of Figure 2, an incremental-decremental curve is added to show the exploitation and exploration abilities of DDRIME, DERIME, DFRIME, and RIME. The balance and diversity analysis of F1, F3, F5, F7, F17, F18, F21, and F22 is presented in Figure 2. Red curve illustrates the exploration phase, while the blue line indicates the exploitation phase. A green line stands for the incremental-decremental trend. The results demonstrate that DDRIME has a larger exploration search ratio than RIME. If the local search is less than or equal to the global search, the green line trends upward. Conversely, if the local search exceeds the global search, the green line trends downward. Ranging from low to high, it illustrates the continuous impact of either local or global exploration efficiency. The introduction of a dispersed foraging mechanism makes the functional test of DDRIME have better detection value than the traditional RIME, showing a comprehensive exploration capacity.

Performance of advanced methods

In the study, DDRIME is compared to ensemble sinusoidal parameter adaptation incorporated with l-shade (LSHADE_cnEpSi), differential evolution algorithm with ensemble of parameters and mutation strategies (EPSDE), differential evolution with linear population size reduction (LSHADE), differential evolution with success-history based parameter adaptation (SADE), adaptive levy-assisted salp swarm algorithm (WLSSA), weighted mean of vectors (INFO), hunger games search (HGS), slime mould algorithm (SMA), augmented Lagrange

Table 3. Laboratory test results such as routine blood biochemistry in the group with successful and unsuccessful invasive mechanical ventilation

Index	Successful mechanical ventilation group (n = 46)	Mechanical ventilation failure group (n = 38)	p value
Age	75.00 (66.00–83.00)	76.50 (69.25–81.25)	0.978
TP	58.67 ± 6.79	57.16 ± 7.69	0.342
ALB	29.96 ± 4.49	30.22 ± 4.58	0.796
TC	3.76 ± 1.00	4.16 ± 1.23	0.112
CPR	32.30 (7.55–87.60)	42.80 (17.30–90.00)	0.182
FIB	4.63 (3.30–6.59)	3.98 (3.09–5.48)	0.148
BNP	329.50 (139.75–841.68)	306.50 (149.25–1532.25)	0.497
BR	9.00 (7.75–12.25)	10.50 (7.00–15.00)	0.551
SCR	74.00 (53.25–102.50)	79.50 (53.50–150.50)	0.719
PMA	31.12 (23.09–40.73)	23.01 (16.66–28.96)	0.000
D-D	1.46 (0.89–2.41)	1.99 (1.38–3.50)	0.035

constrained particle swarm optimization (ALCPSO), improved grey wolf optimizer (IGWO), and dispersed foraging slime mould algorithm (DFSMA) on 60 test functions to further validate the optimization performance. By evaluating the magnitudes in the function optimization test, we demonstrate that DDRIME is most likely to identify the optimal solution. Table 7 describes the results comparing DDRIME with 11 advanced methods, providing mean value (*AVG*) and standard deviation (*STD*) gained from 60 independent tests.

In a word, DDRIME demonstrates the top-ranked optimization performance on the 60 functions and achieves the best solutions in the majority of cases consistently. DDRIME ranks the best for optimal performance on the 60 benchmark functions, consistently providing the optimal solutions in the majority of cases. In addition, based on the statistical test results, it is DDRIME that performs the best on 60 test functions, with only a few functions performing worse than some other algorithms. This effectively validates the "there is no such thing as a free lunch" theorem since no single algorithm can perform the best in all optimization problems. The figure clearly shows that DDRIME attains notably greater convergence accuracy and a quicker convergence rate compared to other methods. Moreover, the algorithm's proficiency in evading local optima is also shown.

In summary, the comparison with 11 well-known methods validates that DDRIME shows excellent performance on the 60 benchmark functions test. Additionally, it demonstrates that dispersed foraging and differential crossover operators significantly increase RIME's ability to identify the optimal solution and help agents avoid local optima.

The DDRIME-based KNN

The continuous DDRIME mentioned was adapted to a binary discrete version using a suitable transfer function (TF) to select a feature subset. One sample was used as the test set to demonstrate the classification accuracy, while the remaining samples were used as the training set. Based on KNN for feature selection, the field size k was set to 1. For fairness, all methods were executed on a main function with identical population initialization. The main function's parameters were as follows: a population size of 20, a fold value of 10, and a maximum of 50 evaluations. All the methods were conducted by the same software on the same hardware equipment.

Comparison of several public datasets

Besides, compared with other methods, several high-dimensional gene datasets were adopted. To evaluate the efficiency of the bDDRIME_KNN model for feature selection, 12 datasets were used, which are presented in Table 8. We have included a brief description of the 12 datasets, as well as citations for the specific datasets mentioned[53]: Brain_Tumor2, DLBCL, SRBCT, Ionosphere, Leukemia, Leukemia1,

Table 4. Variants of RIME with mechanisms

Variants	Improvement mechanism	
	DF	DE
DDRIME	√	√
DFRIME	√	×
DERIME	×	√
RIME	×	×

Table 5. Comparative average and standard deviation values for different variants

Function	Metric	DDRIME	DFRIME	DERIME	RIME
F1	*AVG*	1.8601E-71	9.7142E-22	**8.7941E-72**	4.3819E-04
	SD	5.0256E-71	1.1875E-21	**2.4145E-71**	3.0551E-04
F2	*AVG*	4.2533E-41	2.9640E-11	**3.4600E-43**	1.4370E-02
	SD	2.7214E-41	1.8114E-11	**3.1357E-43**	6.6533E-03
F3	*AVG*	**4.8862E-04**	6.2082E-04	8.0676E-02	1.1897E+00
	SD	**3.8471E-04**	8.1996E-04	4.0372E-02	3.6622E-01
F4	*AVG*	2.6710E-03	1.3365E-02	**4.1087E-06**	1.1519E-01
	SD	3.5564E-03	5.9790E-03	**2.1125E-05**	4.4109E-02
F5	*AVG*	**1.0811E+01**	1.8073E+01	4.8424E+01	1.1551E+02
	SD	1.9452E+01	**1.8953E+01**	3.1515E+01	1.0762E+02
F6	*AVG*	**0.0000E+00**	5.5039E-22	**0.0000E+00**	3.6366E-04
	SD	**0.0000E+00**	7.8575E-22	**0.0000E+00**	1.8794E-04
F7	*AVG*	**1.4449E-03**	2.3381E-03	1.5679E-03	2.9493E-03
	SD	**4.9995E-04**	9.1282E-04	6.7735E-04	9.1644E-04
F8	*AVG*	−1.2222E+04	−1.1956E+04	**−1.2277E+04**	−1.1750E+04
	SD	1.6746E+02	1.8558E+02	**1.3831E+02**	2.9231E+02
F9	*AVG*	8.8883E+00	1.3498E+01	**7.3959E+00**	1.0381E+01
	SD	3.1019E+00	3.1537E+00	**2.4327E+00**	2.8346E+00
F10	*AVG*	**6.2172E-15**	4.3899E-12	7.8752E-15	4.3867E-03
	SD	1.8067E-15	2.6642E-12	**6.4863E-16**	1.3357E-03
F11	*AVG*	**0.0000E+00**	1.3970E-03	**0.0000E+00**	1.0787E-02
	SD	**0.0000E+00**	3.2165E-03	**0.0000E+00**	1.1985E-02
F12	*AVG*	**1.5705E-32**	2.4581E-24	**1.5705E-32**	1.5564E-06
	SD	**5.5674E-48**	3.7182E-24	**5.5674E-48**	6.3357E-07
F13	*AVG*	**1.3498E-32**	1.2053E-22	**1.3498E-32**	2.2219E-03
	SD	**5.5674E-48**	2.6974E-22	**5.5674E-48**	4.4756E-03
F14	*AVG*	**9.9800E-01**	**9.9800E-01**	**9.9800E-01**	9.9800E-01
	SD	**1.1662E-16**	2.2395E-16	2.7813E-16	1.4481E-15
F15	*AVG*	5.2115E-04	**4.2958E-04**	2.4085E-03	5.7218E-03
	SD	3.9391E-04	**3.1660E-04**	6.0935E-03	8.9836E-03
F16	*AVG*	**−1.0316E+00**	**−1.0316E+00**	**−1.0316E+00**	**−1.0316E+00**
	SD	**6.7752E-16**	**6.7752E-16**	**6.7752E-16**	7.4589E-11
F17	*AVG*	**3.9789E-01**	**3.9789E-01**	**3.9789E-01**	3.9789E-01
	SD	**0.0000E+00**	**0.0000E+00**	3.2434E-16	2.4601E-10
F18	*AVG*	**3.0000E+00**	**3.0000E+00**	**3.0000E+00**	**3.0000E+00**
	SD	**1.1216E-15**	2.1789E-12	6.9271E-15	4.0928E-10
F19	*AVG*	**−3.8628E+00**	**−3.8628E+00**	**−3.8628E+00**	−3.8628E+00
	SD	**2.7101E-15**	**2.7101E-15**	**2.7101E-15**	3.6359E-10
F20	*AVG*	**−3.3220E+00**	**−3.3220E+00**	**−3.3220E+00**	−3.3141E+00
	SD	**1.3297E-15**	**1.3297E-15**	1.3424E-15	3.0164E-02
F21	*AVG*	**−1.0153E+01**	**−1.0153E+01**	−9.9848E+00	−9.8164E+00
	SD	**7.2269E-15**	**7.2269E-15**	9.2244E-01	1.2818E+00
F22	*AVG*	**−1.0403E+01**	**−1.0403E+01**	**−1.0403E+01**	−1.0403E+01
	SD	1.8067E-15	**1.4752E-15**	1.7764E-15	4.2718E-07
F23	*AVG*	**−1.0536E+01**	**−1.0536E+01**	**−1.0536E+01**	−1.0536E+01

(*Continued on next page*)

Table 5. *Continued*

Function	Metric	DDRIME	DFRIME	DERIME	RIME
	SD	**1.6160E-15**	1.8067E-15	1.7455E-15	4.1745E-07
F24	*AVG*	2.9007E+05	**1.9976E+05**	1.3297E+06	2.6566E+06
	SD	1.5511E+05	**1.1785E+05**	7.2949E+05	9.4451E+05
F25	*AVG*	**2.0000E+02**	2.0000E+02	4.9997E+03	1.0536E+04
	SD	**1.0556E-14**	1.1073E-07	7.3560E+03	1.1312E+04
F26	*AVG*	**3.0000E+02**	3.0000E+02	3.2315E+02	3.3471E+02
	SD	**3.5009E-14**	8.1115E-09	2.0538E+01	2.4013E+01
F27	*AVG*	**4.1850E+02**	4.2106E+02	4.6037E+02	4.9009E+02
	SD	**2.9648E+01**	3.1402E+01	4.1877E+01	3.2535E+01
F28	*AVG*	5.2004E+02	**5.2001E+02**	5.2003E+02	5.2002E+02
	SD	3.8778E-02	**1.4577E-02**	4.4356E-02	3.6368E-02
F29	*AVG*	6.0842E+02	6.0966E+02	**6.0803E+02**	6.1224E+02
	SD	3.0249E+00	3.3724E+00	**2.7274E+00**	2.8164E+00
F30	*AVG*	7.0000E+02	7.0000E+02	**7.0000E+02**	7.0002E+02
	SD	1.5645E-11	1.3503E-03	**1.7151E-13**	1.2452E-02
F31	*AVG*	8.0998E+02	8.1214E+02	**8.0803E+02**	8.1005E+02
	SD	**2.5665E+00**	3.5864E+00	2.8375E+00	2.6563E+00
F32	*AVG*	**9.5036E+02**	9.6130E+02	9.5782E+02	9.8049E+02
	SD	**1.1139E+01**	1.3356E+01	1.6633E+01	1.7497E+01
F33	*AVG*	**1.2873E+03**	1.4016E+03	1.3057E+03	1.4070E+03
	SD	2.1423E+02	2.1481E+02	2.1626E+02	**1.6089E+02**
F34	*AVG*	3.6199E+03	**3.5975E+03**	3.7869E+03	3.6792E+03
	SD	4.9217E+02	4.1883E+02	5.6428E+02	**3.9123E+02**
F35	*AVG*	**1.2001E+03**	1.2001E+03	1.2002E+03	1.2002E+03
	SD	4.8793E-02	**4.8630E-02**	9.2089E-02	1.1146E-01
F36	*AVG*	**1.3002E+03**	1.3003E+03	1.3002E+03	1.3004E+03
	SD	5.5535E-02	6.1950E-02	**5.5494E-02**	8.2390E-02
F37	*AVG*	**1.4003E+03**	1.4003E+03	1.4003E+03	1.4003E+03
	SD	**4.1032E-02**	1.2695E-01	1.2882E-01	1.7253E-01
F38	*AVG*	**1.5039E+03**	1.5042E+03	1.5042E+03	1.5062E+03
	SD	**9.8454E-01**	1.2019E+00	1.2010E+00	2.2248E+00
F39	*AVG*	**1.6101E+03**	1.6107E+03	1.6105E+03	1.6112E+03
	SD	6.1360E-01	6.0834E-01	**5.9736E-01**	7.9505E-01
F40	*AVG*	4.0989E+03	**3.0723E+03**	2.9794E+05	2.1518E+05
	SD	2.1102E+03	**6.0649E+02**	2.0331E+05	1.2226E+05
F41	*AVG*	1.9465E+03	**1.9100E+03**	5.4468E+03	5.6641E+03
	SD	6.4735E+02	**2.2651E+02**	3.5681E+03	4.4677E+03
F42	*AVG*	**1.9059E+03**	1.9069E+03	1.9123E+03	1.9248E+03
	SD	1.7029E+00	**1.3922E+00**	1.7694E+01	3.2861E+01
F43	*AVG*	**2.0146E+03**	2.0415E+03	2.0407E+03	2.0873E+03
	SD	**5.0918E+00**	1.9143E+01	2.7014E+01	3.2462E+01
F44	*AVG*	**2.4565E+03**	2.5670E+03	1.0131E+05	1.0723E+05
	SD	2.0382E+02	**1.5826E+02**	6.8192E+04	8.6069E+04
F45	*AVG*	**2.4222E+03**	2.4448E+03	2.4947E+03	2.5140E+03
	SD	1.1907E+02	**1.1021E+02**	1.5817E+02	1.4258E+02

(*Continued on next page*)

Table 5. *Continued*

Function	Metric	DDRIME	DFRIME	DERIME	RIME
F46	*AVG*	**2.6152E+03**	**2.6152E+03**	**2.6152E+03**	2.6152E+03
	SD	**1.3876E-12**	2.1743E-12	**1.3876E-12**	3.0965E-03
F47	*AVG*	2.6270E+03	2.6278E+03	**2.6269E+03**	2.6304E+03
	SD	**3.6777E+00**	5.4362E+00	4.4958E+00	6.0206E+00
F48	*AVG*	**2.7040E+03**	2.7045E+03	2.7053E+03	2.7071E+03
	SD	**8.7574E-01**	1.3152E+00	1.6584E+00	2.0832E+00
F49	*AVG*	**2.7002E+03**	2.7036E+03	2.7036E+03	2.7070E+03
	SD	**3.3210E-02**	1.8220E+01	1.8240E+01	2.5337E+01
F50	*AVG*	**3.1368E+03**	3.1375E+03	3.1736E+03	3.3196E+03
	SD	**6.4709E+01**	7.1903E+01	9.2861E+01	1.4760E+02
F51	*AVG*	**3.6506E+03**	3.6575E+03	3.6704E+03	3.8073E+03
	SD	5.6426E+01	**5.0374E+01**	6.1307E+01	2.0842E+02
F52	*AVG*	2.8379E+05	**3.7342E+03**	4.5983E+03	5.9799E+05
	SD	1.5339E+06	**1.5719E+02**	5.9369E+02	2.2592E+06
F53	*AVG*	5.1089E+03	**4.7897E+03**	5.9969E+03	6.6131E+03
	SD	8.5169E+02	1.0121E+03	**7.9102E+02**	1.1739E+03
F54	*AVG*	**1.0000E+02**	1.0000E+02	3.2677E+03	4.9254E+03
	SD	**1.2093E-14**	8.9509E-04	4.1977E+03	5.2872E+03
F55	*AVG*	2.0490E+02	2.3097E+02	**2.0000E+02**	2.1801E+02
	SD	9.3164E+00	1.3625E+02	**1.0677E-04**	3.3551E+01
F56	*AVG*	**3.0002E+02**	3.0006E+02	3.0031E+02	3.0118E+02
	SD	**1.7696E-02**	4.4800E-02	1.6592E-01	6.2750E-01
F57	*AVG*	4.4022E+02	**4.3344E+02**	4.8149E+02	4.8267E+02
	SD	2.7530E+01	3.3683E+01	2.2956E+01	**2.2177E+01**
F58	*AVG*	**5.5205E+02**	5.5733E+02	5.5424E+02	5.7637E+02
	SD	**1.0644E+01**	1.2216E+01	1.2607E+01	1.9672E+01
F59	*AVG*	**6.0000E+02**	6.0005E+02	**6.0000E+02**	6.0041E+02
	SD	**0.0000E+00**	1.0517E-01	4.7206E-14	5.9418E-01
F60	*AVG*	**7.7317E+02**	7.9079E+02	7.7917E+02	8.0735E+02
	SD	1.3062E+01	**1.2027E+01**	1.4189E+01	2.1085E+01
F61	*AVG*	**8.5255E+02**	8.5701E+02	8.5334E+02	8.8500E+02
	SD	**9.6277E+00**	1.2652E+01	1.4941E+01	1.9894E+01
F62	*AVG*	**9.0126E+02**	9.1282E+02	9.0136E+02	1.3384E+03
	SD	3.9160E+00	1.8030E+01	**2.5690E+00**	6.4239E+02
F63	*AVG*	3.8273E+03	**3.6933E+03**	3.8400E+03	3.8373E+03
	SD	**4.6156E+02**	5.8965E+02	6.1400E+02	6.3550E+02
F64	*AVG*	**1.1384E+03**	1.1587E+03	1.1389E+03	1.1752E+03
	SD	2.3803E+01	3.0441E+01	**2.3707E+01**	3.1583E+01
F65	*AVG*	**1.2627E+04**	1.3635E+04	3.1720E+05	2.4220E+06
	SD	**1.1929E+04**	1.2239E+04	2.8972E+05	1.5504E+06
F66	*AVG*	**1.3678E+03**	5.7340E+03	2.2338E+04	1.6538E+04
	SD	**1.8817E+01**	1.5438E+04	2.1837E+04	1.7765E+04
F67	*AVG*	**1.4363E+03**	1.4442E+03	1.3091E+04	1.1660E+04
	SD	**4.7852E+00**	9.6610E+00	8.2575E+03	6.5395E+03
F68	*AVG*	**1.5238E+03**	1.5835E+03	1.0131E+04	1.2820E+04

(*Continued on next page*)

Table 5. *Continued*

Function	Metric	DDRIME	DFRIME	DERIME	RIME
	SD	**1.7042E+01**	3.4290E+01	1.0832E+04	1.3566E+04
F69	*AVG*	**2.0205E+03**	2.0472E+03	2.1895E+03	2.3726E+03
	SD	**2.0356E+02**	2.1399E+02	2.4084E+02	2.3479E+02
F70	*AVG*	**1.8226E+03**	1.8772E+03	1.9057E+03	2.0749E+03
	SD	**9.1160E+01**	1.0709E+02	1.2328E+02	1.6603E+02
F71	*AVG*	**1.8741E+03**	1.8855E+03	2.3605E+05	2.9805E+05
	SD	3.6741E+01	**2.7084E+01**	1.8125E+05	2.8034E+05
F72	*AVG*	**1.9150E+03**	1.9273E+03	1.3923E+04	1.3290E+04
	SD	**2.7037E+00**	7.2848E+00	1.1474E+04	1.3010E+04
F73	*AVG*	**2.1724E+03**	2.1863E+03	2.2346E+03	2.3209E+03
	SD	**8.7555E+01**	9.0518E+01	1.1882E+02	1.5443E+02
F74	*AVG*	**2.3497E+03**	2.3627E+03	2.3539E+03	2.3877E+03
	SD	**9.6511E+00**	1.2206E+01	1.2133E+01	1.6062E+01
F75	*AVG*	**3.0052E+03**	3.6361E+03	3.6423E+03	4.1611E+03
	SD	**1.3323E+03**	1.4843E+03	1.7228E+03	1.4772E+03
F76	*AVG*	2.7088E+03	2.7119E+03	**2.7078E+03**	2.7401E+03
	SD	**1.4809E+01**	1.5508E+01	2.0693E+01	2.2412E+01
F77	*AVG*	**2.8790E+03**	2.8919E+03	2.9031E+03	2.9129E+03
	SD	**1.4327E+01**	2.1212E+01	1.8021E+01	2.0088E+01
F78	*AVG*	**2.8865E+03**	2.8877E+03	2.8875E+03	2.8922E+03
	SD	**1.2329E+00**	7.0240E+00	1.4457E+00	1.1160E+01
F79	*AVG*	**4.1420E+03**	4.2913E+03	4.2957E+03	4.7083E+03
	SD	3.7964E+02	3.4288E+02	**1.4508E+02**	2.9169E+02
F80	*AVG*	**3.2043E+03**	3.2053E+03	3.2106E+03	3.2236E+03
	SD	**5.0491E+00**	8.4047E+00	7.8013E+00	1.6272E+01
F81	*AVG*	3.1685E+03	**3.1353E+03**	3.1934E+03	3.2099E+03
	SD	5.7934E+01	4.9897E+01	6.5046E+01	**4.4007E+01**
F82	*AVG*	**3.4070E+03**	3.5456E+03	3.4961E+03	3.6656E+03
	SD	**8.0357E+01**	9.5470E+01	1.1232E+02	1.5435E+02
F83	*AVG*	**5.3386E+03**	5.4752E+03	1.0132E+04	1.6258E+04
	SD	**3.2019E+02**	4.4161E+02	4.1706E+03	1.1750E+04

Leukemia2, penglung, Prostate_Tumor, Lung_Cancer, Tumors_11, and Tumors_14. This additional information will enhance the clarity and comprehensiveness of our work.

Traditional and state-of-the-art methods are taken as a comparison with the bDDRIME_KNN model. In this section, bDDRIME is compared with 11 algorithms, including bSMA, bHGS, bHHO, bRUN, bIGWO, bDFSMA, bISMA, bAOA, bINFO, bGBO, and bRIME. The initialization of the primary feature in the 12 datasets is set to values between −1 and 1. Following established rules in the renowned machine learning literature,[55,56] we use a 10-fold cross-validation(CV) to obtain unbiased and accurate results. The statistical outcomes, including several selected features, classification error rate, comparison time cost, and best fitness values are presented in Tables 8, 9, 10, and 11.

Tables 8, 9, and 10 present that bDDRIME is superior to other versions in terms of mean error rate, mean fitness value, and mean number of selected features. The bDDRIME_KNN model ranks first and can find the most suitable subsets of features across 12 datasets. Therefore, it is crucial to select a subset of the optimal number. Here, the bDDRIME_KNN model ranks first on average among the mentioned methods. The optimal fitness gained by the KNN classifier from the running method is graphically described as a curve, which intuitively shows the advantage of the bDDRIME_KNN model in feature selection. This ensures that the optimal candidate is chosen. The dispersed foraging mechanism periodically reassigns population agents to the best positions, preventing them from becoming trapped in local optima, while the differential crossover operator enhances convergence and accelerates local search capabilities.

The size of the dataset and the algorithm's ability to converge influence the method's speed. As shown in Table 11, the bDDRIME_KNN model needs more execution time than traditional methods due to the addition search operator of dispersed foraging and differential crossover.

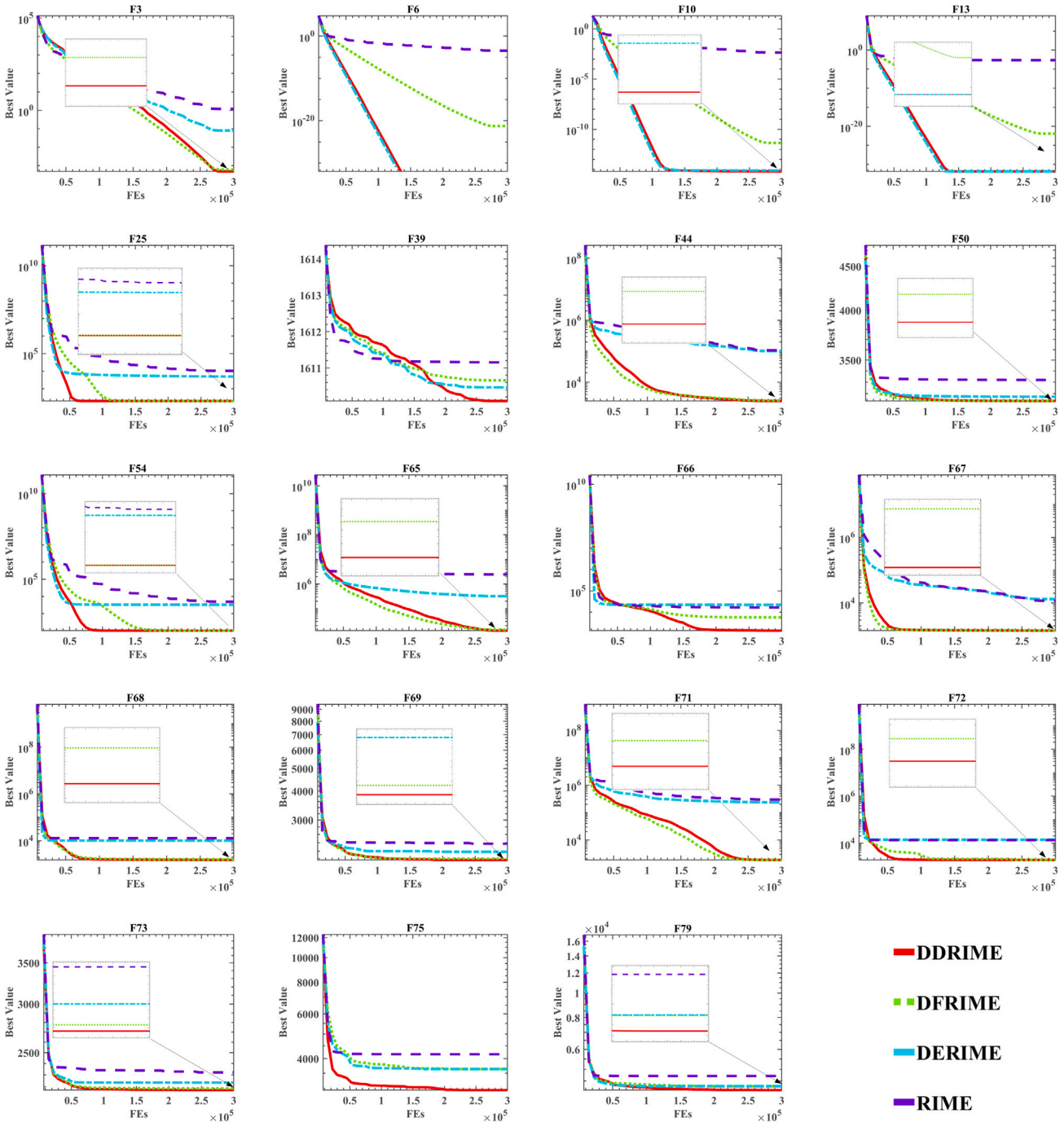

Figure 1. Convergence curves of different RIME methods

Figure 3 shows the best score so far of the bDDRIME fitness on 12 datasets. In contrast, it can be seen that the difference between the bRIME and other methods is significant on 12 datasets. The bDDRIME method with excellent performance finds a perfect value at startup temporarily and evaluates the individual's fitness when it updates position. It guarantees the selection of the top candidates. To avoid slipping into local optimality, dispersed foraging and differential crossover will update population locations with the current optimal to ensure the diversity of algorithms occasionally. The modified mechanisms will improve the algorithm's convergence speed and its ability to mine data effectively.

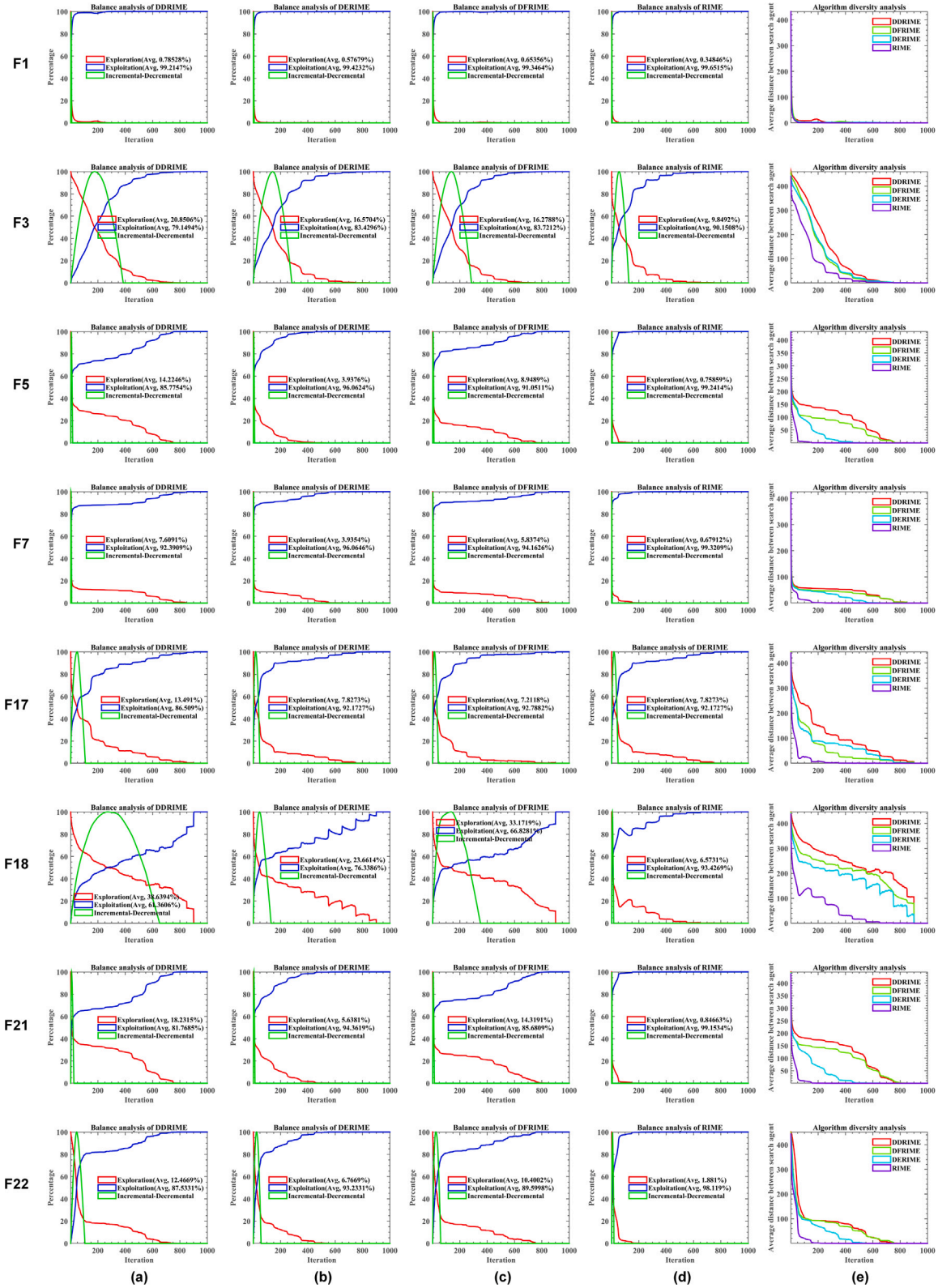

Figure 2. Balance and diversity analysis of the proposed methods

Table 6. *p* values gained by Wilcoxon test

Function	DDRIME	DFRIME	DERIME	RIME
F1	-	1.734E-06	1.064E-01	1.734E-06
F2	-	1.734E-06	1.734E-06	1.734E-06
F3	-	5.577E-01	1.734E-06	1.734E-06
F4	-	5.7522E-06	1.921E-06	1.734E-06
F5	-	6.639E-04	1.921E-06	4.729E-06
F6	-	1.734E-06	1.000E+00	1.734E-06
F7	-	2.831E-04	4.908E-01	2.603E-06
F8	-	7.196E-05	2.475E-01	2.879E-06
F9	-	2.956E-05	6.598E-02	1.566E-02
F10	-	1.732E-06	1.221E-04	1.734E-06
F11	-	1.953E-03	1.000E+00	1.734E-06
F12	-	1.734E-06	1.000E+00	1.734E-06
F13	-	1.734E-06	1.000E+00	1.734E-06
F14	-	2.148E-02	3.906E-02	1.977E-07
F15	-	5.431E-01	1.747E-01	8.188E-05
F16	-	1.000E+00	1.000E+00	1.734E-06
F17	-	1.000E+00	1.000E+00	1.734E-06
F18	-	1.763E-04	1.242E-04	1.734E-06
F19	-	1.000E+00	1.000E+00	1.734E-06
F20	-	1.000E+00	1.000E+00	1.734E-06
F21	-	1.000E+00	1.000E+00	1.734E-06
F22	-	1.000E+00	1.000E+00	1.734E-06
F23	-	1.000E+00	1.000E+00	1.734E-06
F24	-	1.108E-02	1.921E-06	1.734E-06
F25	-	1.734E-06	1.734E-06	1.734E-06
F26	-	1.734E-06	1.734E-06	1.734E-06
F27	-	7.655E-01	2.597E-05	2.353E-06
F28	-	1.593E-03	4.048E-01	1.064E-01
F29	-	1.779E-01	5.999E-01	3.317E-04
F30	-	2.915E-05	1.250E-01	1.734E-06
F31	-	9.714E-03	1.169E-02	4.6528E-01
F32	-	9.627E-04	5.446E-02	5.2165E-06
F33	-	8.590E-02	9.263E-01	1.2453E-02
F34	-	7.813E-01	1.254E-01	7.9710E-01
F35	-	4.780E-01	1.175E-02	1.7988E-05
F36	-	5.710E-02	4.653E-01	8.4661E-06
F37	-	6.733E-01	2.415E-03	6.8359E-03
F38	-	5.038E-01	4.405E-01	4.8603E-05
F39	-	8.944E-04	3.001E-02	1.2381E-05
F40	-	4.992E-03	1.734E-06	1.7344E-06
F41	-	5.307E-05	1.127E-05	1.9209E-06
F42	-	2.703E-02	3.001E-02	2.1266E-06
F43	-	1.921E-06	3.515E-06	1.7344E-06
F44	-	6.268E-02	1.734E-06	1.7344E-06
F45	-	2.536E-01	4.716E-02	1.5658E-02

(*Continued on next page*)

Table 6. *Continued*

Function	DDRIME	DFRIME	DERIME	RIME
F46	-	5.000E-01	1.000E+00	1.7344E-06
F47	-	7.189E-01	5.440E-01	4.2767E-02
F48	-	5.193E-02	3.317E-04	3.5152E-06
F49	-	2.703E-02	6.319E-05	1.7344E-06
F50	-	5.304E-01	1.064E-01	4.2857E-06
F51	-	7.971E-01	1.470E-01	1.1499E-04
F52	-	5.999E-01	5.792E-05	4.8603E-05
F53	-	1.204E-01	1.709E-03	2.3704E-05
F54	-	1.734E-06	1.734E-06	1.7344E-06
F55	-	1.109E-01	9.263E-01	1.6566E-02
F56	-	2.052E-04	1.734E-06	1.7344E-06
F57	-	2.536E-01	3.405E-05	1.4936E-05
F58	-	4.949E-02	8.130E-01	2.5967E-05
F59	-	1.734E-06	1.000E+00	1.7344E-06
F60	-	6.892E-05	1.254E-01	5.2165E-06
F61	-	1.020E-01	9.589E-01	5.2165E-06
F62	-	1.038E-04	1.240E-01	1.7344E-06
F63	-	3.185E-01	8.774E-01	9.7539E-01
F64	-	2.067E-02	5.857E-01	1.8910E-04
F65	-	6.288E-01	1.734E-06	1.7344E-06
F66	-	1.734E-06	1.734E-06	1.7344E-06
F67	-	9.711E-05	1.734E-06	1.7344E-06
F68	-	2.127E-06	1.921E-06	1.7344E-06
F69	-	7.499E-01	2.958E-03	1.1265E-05
F70	-	1.657E-02	1.479E-02	6.9838E-06
F71	-	3.683E-02	1.734E-06	1.7344E-06
F72	-	2.127E-06	1.734E-06	1.7344E-06
F73	-	8.774E-01	4.716E-02	2.2248E-04
F74	-	1.477E-04	2.369E-01	1.9209E-06
F75	-	7.271E-03	8.402E-02	1.4839E-03
F76	-	2.210E-01	7.655E-01	2.603E-06
F77	-	1.957E-02	1.799E-05	6.984E-06
F78	-	2.369E-01	4.897E-04	5.706E-04
F79	-	1.479E-02	4.4920E-02	4.729E-06
F80	-	5.999E-01	1.382E-03	5.217E-06
F81	-	2.067E-02	2.134E-01	6.639E-04
F82	-	7.514E-05	4.682E-03	5.217E-06
F83	-	1.204E-01	1.734E-06	1.734E-06
+/−/=	/	41/5/37	39/4/40	79/0/4
ARV	1.301205	2.192771	2.325301	3.86747
Rank	1	2	3	4

Experiment on the AECOPD dataset

To illustrate the performance of the bDDRIME_KNN model on the AECOPD dataset, it is compared with six commonly used classifiers by time, accuracy (*ACC*), specificity, precision, Matthews correlation coefficients (*MCCs*), and F-measure. The results prove that bDDRIME_KNN compares against other classifiers in five performance metrics. Although the time cost of the proposed bDDRIME_KNN is more than others, the values of *ACC*, specificity, precision, *MCC*, and F-measure are higher than others.

Table 7. Comparative results with the mentioned algorithms

Function	Metric	DDRIME	LSHADE_cnEpSi	EPSDE	LSHADE	SADE	WLSSA	INFO	HGS	SMA	ALCPSO	IGWO	DFSMA
F24	*AVG*	2.624E+05	4.590E+03	1.238E+05	**3.528E+03**	4.552E+05	3.919E+06	2.742E+04	2.617E+06	2.111E+06	5.903E+06	1.585E+07	5.119E+04
	SD	1.692E+05	**3.339E+03**	6.552E+05	6.908E+03	4.469E+05	1.481E+06	2.569E+04	4.762E+06	8.784E+05	6.407E+06	5.205E+06	4.044E+04
F25	*AVG*	**2.000E+02**	2.000E+02	**2.000E+02**	**2.000E+02**	2.000E+02	8.865E+03	2.000E+02	1.178E+04	1.261E+04	2.766E+03	2.697E+06	2.000E+02
	SD	**1.056E-14**	4.819E-09	1.117E-13	4.255E-14	2.209E-08	8.186E+03	2.435E-06	1.403E+04	1.202E+04	3.703E+03	1.265E+06	6.962E-07
F26	*AVG*	**3.000E+02**	3.000E+02	3.000E+02	3.000E+02	4.297E+02	1.417E+04	3.000E+02	7.099E+03	3.849E+02	4.338E+02	6.673E+03	3.000E+02
	SD	**3.9495E-14**	2.046E-12	2.597E-10	1.934E-12	3.036E+02	4.278E+03	4.039E-06	3.656E+03	1.143E+02	3.584E+02	2.268E+03	1.194E-06
F27	*AVG*	4.143E+02	4.115E+02	4.108E+02	**4.077E+02**	4.353E+02	5.091E+02	4.099E+02	5.038E+02	5.053E+02	5.265E+02	5.310E+02	4.084E+02
	SD	2.689E+01	3.345E+01	**5.302E+00**	2.002E+01	3.939E+01	4.460E+01	2.387E+01	3.410E+01	3.411E+01	5.596E+01	2.652E+01	1.959E+01
F28	*AVG*	5.201E+02	**5.200E+02**	5.203E+02	5.200E+02	5.205E+02	5.201E+02	5.202E+02	5.200E+02	5.208E+02	5.208E+02	5.205E+02	5.208E+02
	SD	5.685E-02	**7.585E-03**	2.989E-02	4.656E-02	4.946E-02	1.262E-01	1.280E-01	5.280E-02	1.502E-01	5.762E-02	1.334E-01	6.561E-02
F29	*AVG*	**6.081E+02**	6.119E+02	6.177E+02	6.117E+02	6.084E+02	6.129E+02	6.221E+02	6.176E+02	6.159E+02	6.174E+02	6.189E+02	6.114E+02
	SD	3.353E+00	2.746E+00	2.513E+00	2.720E+00	**2.366E+00**	3.869E+00	3.562E+00	2.968E+00	2.569E+00	3.554E+00	3.592E+00	3.872E+00
F30	*AVG*	**7.000E+02**	7.000E+02	7.000E+02	7.000E+02	7.000E+02	7.000E+02	7.001E+02	7.000E+02	7.003E+02	7.000E+02	7.009E+02	7.000E+02
	SD	**9.364E-11**	1.518E-02	1.255E-02	1.201E-02	1.879E-02	9.515E-03	1.756E-01	2.485E-02	9.556E-02	1.759E-02	1.105E-01	8.406E-05
F31	*AVG*	8.111E+02	8.026E+02	8.000E+02	**8.000E+02**	8.015E+02	9.243E+02	9.071E+02	8.042E+02	8.109E+02	8.202E+02	8.788E+02	8.349E+02
	SD	3.464E+00	2.226E+00	1.816E-01	**2.058E-13**	1.425E+00	2.782E+01	2.428E+01	5.029E+00	3.008E+00	7.319E+00	1.423E+01	8.249E+00
F32	*AVG*	9.468E+02	9.384E+02	9.403E+02	**9.326E+02**	9.468E+02	1.051E+03	1.038E+03	1.022E+03	9.979E+02	1.003E+03	1.012E+03	9.709E+02
	SD	1.221E+01	**6.1487E+00**	1.121E+01	7.461E+00	1.247E+01	3.075E+01	3.142E+01	2.719E+01	3.034E+01	2.970E+01	1.663E+01	1.653E+01
F33	*AVG*	1.341E+03	1.092E+03	**1.001E+03**	1.0162E+03	1.002E+03	4.019E+03	2.924E+03	1.238E+03	1.609E+03	1.544E+03	3.323E+03	2.083E+03
	SD	1.644E+02	8.034E+01	**1.034E+00**	4.084E+01	2.058E+00	8.112E+02	5.956E+02	1.445E+02	1.729E+02	2.438E+02	6.323E+02	3.501E+02
F34	*AVG*	3.624E+03	**2.656E+03**	4.444E+03	2.890E+03	3.054E+03	4.693E+03	4.950E+03	3.795E+03	4.119E+03	4.145E+03	4.237E+03	3.882E+03
	SD	5.786E+02	**2.634E+02**	7.726E+02	2.961E+02	5.355E+02	5.844E+02	6.331E+02	4.824E+02	5.685E+02	5.986E+02	6.219E+02	4.317E+02
F35	*AVG*	**1.200E+03**	**1.200E+03**	1.201E+03	1.200E+03	1.200E+03	1.200E+03	1.200E+03	1.200E+03	1.200E+03	1.202E+03	1.201E+03	1.201E+03
	SD	6.016E-02	**2.189E-02**	7.645E-02	5.076E-02	9.058E-02	2.149E-01	1.657E-01	5.406E-02	1.226E-01	4.759E-01	2.936E-01	2.798E-01
F36	*AVG*	**1.300E+03**	1.300E+03	1.300E+03	1.300E+03	1.300E+03	1.3005E+03	1.301E+03	1.301E+03	1.300E+03	1.301E+03	1.301E+03	1.300E+03
	SD	5.428E-02	8.495E-02	**4.652E-02**	7.510E-02	4.714E-02	1.1562E-01	1.143E-01	9.021E-02	1.208E-01	8.929E-02	1.397E-01	4.827E-02
F37	*AVG*	1.400E+03	1.400E+03	1.400E+03	1.400E+03	**1.400E+03**	1.4003E+03	1.400E+03	1.401E+03	1.401E+03	1.401E+03	1.401E+03	1.400E+03
	SD	8.078E-02	1.009E-01	1.203E-01	1.662E-01	3.766E-02	1.6951E-01	1.744E-01	3.064E-01	2.543E-01	3.166E-01	3.602E-01	**2.769E-02**
F38	*AVG*	**1.504E+03**	1.507E+03	1.506E+03	1.506E+03	1.506E+03	1.5068E+03	1.539E+03	1.511E+03	1.507E+03	1.511E+03	1.518E+03	1.507E+03
	SD	**8.159E-01**	4.051E+00	1.041E+00	2.296E+00	1.625E+00	2.8270E+00	3.804E+01	4.372E+00	1.906E+00	4.594E+00	4.418E+00	1.752E+00
F39	*AVG*	1.610E+03	**1.609E+03**	1.6110E+03	1.6094E+03	1.611E+03	1.612E+03	1.612E+03	1.611E+03	1.611E+03	1.612E+03	1.6114E+03	1.612E+03
	SD	6.495E-01	5.592E-01	**3.939E-01**	6.290E-01	5.215E-01	6.729E-01	5.932E-01	7.509E-01	6.120E-01	5.897E-01	6.543E-01	4.269E-01
F40	*AVG*	3.725E+03	3.407E+03	5.564E+04	3.386E+03	4.557E+04	2.427E+05	7.346E+03	3.858E+05	2.966E+05	6.918E+05	8.498E+05	**2.822E+03**

(*Continued on next page*)

Table 7. *Continued*

Function	Metric	DDRIME	LSHADE_cnEpSi	EPSDE	LSHADE	SADE	WLSSA	INFO	HGS	SMA	ALCPSO	IGWO	DFSMA
	SD	1.279E+03	4.584E+02	6.329E+04	6.108E+02	3.118E+04	1.734E+05	4.620E+03	2.209E+05	1.183E+05	8.091E+05	5.636E+05	**2.641E+02**
F41	*AVG*	2.195E+03	1.952E+03	3.433E+03	1.949E+03	2.845E+03	6.977E+03	5.948E+03	1.324E+04	1.829E+04	7.571E+03	2.279E+04	**1.871E+03**
	SD	1.992E+03	6.824E+01	3.056E+03	7.689E+01	1.388E+03	6.835E+03	5.466E+03	9.629E+03	9.525E+03	6.782E+03	2.928E+04	**1.203E+01**
F42	*AVG*	**1.906E+03**	1.910E+03	1.913E+03	1.908E+03	1.907E+03	1.912E+03	1.914E+03	1.920E+03	1.921E+03	1.917E+03	1.915E+03	1.907E+03
	SD	1.328E+00	2.304E+00	1.091E+00	1.802E+00	1.105E+01	2.134E+00	1.492E+01	2.443E+01	2.845E+01	2.687E+01	2.632E+00	**7.568E-01**
F43	*AVG*	**2.014E+03**	2.284E+03	2.258E+03	2.809E+03	2.668E+03	4.701E+03	2.203E+03	6.256E+03	2.176E+03	3.061E+03	3.728E+03	2.048E+03
	SD	**4.384E+00**	1.102E+02	9.435E+02	2.279E+03	5.272E+02	2.297E+03	8.029E+01	2.716E+03	5.185E+01	5.291E+02	2.014E+03	1.483E+01
F44	*AVG*	**2.437E+03**	3.179E+03	1.246E+04	2.798E+03	2.258E+04	8.741E+04	5.171E+03	2.402E+05	1.506E+05	1.130E+05	2.855E+05	2.711E+03
	SD	1.922E+02	2.915E+02	1.327E+04	2.539E+02	1.819E+04	5.412E+04	2.373E+03	2.269E+05	5.612E+04	2.304E+05	2.522E+05	**1.617E+02**
F45	*AVG*	2.409E+03	2.457E+03	2.439E+03	2.399E+03	**2.342E+03**	2.586E+03	2.802E+03	2.761E+03	2.655E+03	2.609E+03	2.541E+03	2.402E+03
	SD	1.052E+02	1.172E+02	1.002E+02	1.071E+02	**6.746E+01**	1.568E+02	1.969E+02	2.422E+02	1.680E+02	2.057E+02	1.507E+02	9.580E+01
F46	*AVG*	2.615E+03	2.615E+03	2.614E+03	2.615E+03	2.615E+03	**2.500E+03**	**2.500E+03**	**2.500E+03**	**2.500E+03**	2.615E+03	2.620E+03	**2.500E+03**
	SD	1.388E-12	1.782E-01	2.927E-12	2.034E-12	1.335E-12	**0.000E+00**	**0.000E+00**	**0.000E+00**	**0.000E+00**	1.623E-01	1.742E+00	**0.000E+00**
F47	*AVG*	2.628E+03	2.639E+03	2.633E+03	2.642E+03	2.631E+03	**2.600E+03**	**2.600E+03**	2.600E+03	**2.600E+03**	2.638E+03	2.600E+03	**2.600E+03**
	SD	4.305E+00	5.918E+00	7.278E+00	5.025E+00	5.829E+00	**0.000E+00**	**0.000E+00**	1.319E-04	**0.000E+00**	8.211E+00	3.525E-03	**0.000E+00**
F48	*AVG*	2.704E+03	2.708E+03	2.700E+03	2.707E+03	2.712E+03	**2.700E+03**	**2.700E+03**	**2.700E+03**	**2.700E+03**	2.711E+03	2.709E+03	**2.700E+03**
	SD	8.488E-01	3.969E+00	2.369E-01	4.024E+00	1.875E+00	**0.000E+00**	**0.000E+00**	**0.000E+00**	**0.000E+00**	3.713E+00	2.290E+00	**0.000E+00**
F49	*AVG*	**2.700E+03**	2.717E+03	2.700E+03	2.704E+03	2.720E+03	2.701E+03	2.714E+03	2.744E+03	2.701E+03	2.750E+03	2.708E+03	2.700E+03
	SD	5.710E-02	3.775E+01	**5.461E-02**	1.819E+01	4.059E+01	1.273E-01	3.444E+01	5.002E+01	1.318E-01	7.126E+01	1.381E-01	5.944E-02
F50	*AVG*	3.136E+03	3.294E+03	3.479E+03	3.274E+03	3.177E+03	**2.900E+03**	**2.900E+03**	**2.900E+03**	**2.900E+03**	3.492E+03	3.111E+03	**2.900E+03**
	SD	5.973E+01	1.179E+02	1.093E+02	1.055E+02	6.017E+01	**0.000E+00**	**0.000E+00**	**0.000E+00**	**0.000E+00**	2.2715E+02	4.156E+00	**0.000E+00**
F51	*AVG*	3.650E+03	4.047E+03	3.211E+03	3.795E+03	3.731E+03	**3.000E+03**	**3.000E+03**	**3.000E+03**	**3.000E+03**	4.520E+03	3.862E+03	**3.000E+03**
	SD	3.787E+01	2.646E+02	1.592E+01	2.136E+02	4.989E+01	**0.000E+00**	**0.000E+00**	**0.000E+00**	**0.000E+00**	6.836E+02	1.729E+02	**0.000E+00**
F52	*AVG*	5.638E+05	3.708E+03	3.114E+03	3.675E+03	4.108E+03	**3.100E+03**	2.834E+05	4.083E+03	3.928E+03	1.687E+06	3.235E+06	**3.100E+03**
	SD	2.132E+06	4.877E+01	1.316E+00	3.785E+01	2.748E+02	**0.000E+00**	1.534E+06	2.449E+03	1.108E+03	4.310E+06	5.572E+06	**0.000E+00**
F53	*AVG*	4.919E+03	6.123E+03	3.546E+03	5.813E+03	5.108E+03	**3.200E+03**	6.744E+03	3.254E+03	5.522E+03	1.760E+04	2.975E+04	**3.200E+03**
	SD	8.095E+02	1.405E+03	1.406E+02	1.367E+03	6.497E+02	2.159E-12	1.540E+03	2.966E+02	1.349E+03	1.837E+04	1.570E+04	**0.000E+00**
F54	*AVG*	**1.000E+02**	1.000E+02	1.000E+02	**1.000E+02**	2.015E+03	4.876E+03	1.000E+02	4.590E+03	8.241E+03	6.149E+03	1.917E+06	1.000E+02
	SD	**1.119E-14**	1.392E-09	1.183E-09	5.691E-13	2.208E+03	5.939E+03	4.940E-04	2.539E+03	8.509E+03	6.134E+03	9.497E+05	1.413E-02
F55	*AVG*	2.012E +02	2.000E+02	1.604E+14	**2.000E+02**	3.900E+12	4.323E+06	2.000E+02	6.761E+15	2.005E+02	7.046E+17	2.474E+13	8.218E+05
	SD	3.564E+00	3.632E-05	8.785E+14	**5.102E-06**	1.481E+13	1.101E+07	4.774E-04	3.703E+16	2.806E+00	2.194E+18	6.171E+13	2.187E+06
F56	*AVG*	3.000E+02	3.000E+02	7.489E+03	1.182E+04	4.088E+02	**3.000E+02**	3.000E+02	1.245E+03	3.000E+02	2.659E+04	1.269E+03	3.586E+02
	SD	2.774E −02	2.552E-03	2.243E+04	3.056E+04	5.755E+02	**7.515E-10**	3.448E-06	3.741E+03	1.188E-02	3.479E+03	5.734E+02	5.39E+01

(*Continued on next page*)

Table 7. *Continued*

Function	Metric	DDRIME	LSHADE_cnEpSi	EPSDE	LSHADE	SADE	WLSSA	INFO	HGS	SMA	ALCPSO	IGWO	DFSMA
F57	*AVG*	4.463E+02	4.543E+02	**4.118E+02**	4.406E+02	4.454E+02	4.917E+02	4.361E+02	4.804E+02	4.880E+02	5.123E+02	5.036E+02	4.411E+02
	SD	2.994E+01	3.828E+01	1.462E+01	2.823E+01	3.681E+01	1.0818E+01	3.836E+01	2.379E+01	**4.752E+00**	3.341E+01	2.153E+01	3.037E+01
F58	*AVG*	5.488E+02	5.426E+02	5.384E+02	**5.322E+02**	5.424E+02	6.290E+02	6.453E+02	6.247E+02	5.829E+02	6.004E+02	6.086E+02	5.795E+02
	SD	1.307E+01	1.247E+01	**8.028E+00**	8.497E+00	1.025E+01	4.388E+01	3.894E+01	3.227E+01	1.921E+01	2.694E+01	2.831E+01	1.709E+01
F59	*AVG*	**6.000E+02**	6.016E+02	6.000E+02	6.003E+02	6.000E+02	6.228E+02	6.239E+02	6.021E+02	6.009E+02	6.049E+02	6.237E+02	6.017E+02
	SD	**0.000E+00**	1.422E+00	2.970E-02	2.748E-01	4.111E-02	9.888E+00	8.753E+00	2.581E+00	6.635E-01	5.740E+00	6.759E+00	8.196E-01
F60	*AVG*	7.829E+02	7.803E+02	**7.714E+02**	7.768E+02	7.748E+02	8.6409E+02	9.814E+02	8.991E+02	8.278E+02	8.611E+02	8.956E+02	7.995E+02
	SD	1.139E+01	1.543E+01	**7.651E+00**	1.348E+01	1.076E+01	4.477E+01	7.667E+01	4.310E+01	2.077E+01	3.911E+01	3.934E+01	1.386E+01
F61	*AVG*	8.549E+02	8.383E+02	8.417E+02	**8.345E+02**	8.424E+02	9.1591E+02	9.282E+02	9.096E+02	8.976E+02	9.005E+02	8.908E+02	8.661E+02
	SD	1.085E+01	1.129E+01	**7.538E+00**	8.919E+00	1.045E+01	3.199E+01	3.032E+01	2.999E+01	2.297E+01	2.914E+01	2.131E+01	1.606E+01
F62	*AVG*	9.008E+02	1.081E+03	**9.004E+02**	9.846E+02	9.142E+02	3.185E+03	2.984E+03	4.082E+03	1.783E+03	1.833E+03	3.068E+03	9.146E+02
	SD	2.049E+00	1.331E+02	**1.041E+00**	9.203E+01	1.997E+01	1.166E+03	6.437E+02	1.074E+03	8.866E+02	6.917E+02	9.648E+02	1.328E+01
F63	*AVG*	3.743E+03	**2.969E+03**	4.464E+03	3.042E+03	3.183E+03	4.613E+03	5.258E+03	3.889E+03	4.218E+03	4.139E+03	4.762E+03	3.929E+03
	SD	4.838E+02	3.298E+02	5.988E+02	**2.895E+02**	4.644E+02	6.859E+02	6.822E+02	5.089E+02	6.345E+02	5.258E+02	5.082E+02	4.633E+02
F64	*AVG*	**1.130E+03**	1.251E+03	1.143E+03	1.231E+03	1.185E+03	1.236E+03	1.270E+03	1.207E+03	1.247E+03	1.249E+03	1.258E+03	1.148E+03
	SD	**2.212E+01**	5.769E+01	5.054E+01	4.395E+01	3.528E+01	5.288E+01	5.688E+01	3.889E+01	4.922E+01	5.718E+01	2.524E+01	2.2386E+01
F65	*AVG*	1.665E+04	1.106E+04	3.728E+04	9.129E+03	2.736E+04	2.868E+06	1.769E+04	1.173E+06	1.592E+06	3.621E+05	1.645E+07	**3.535E+03**
	SD	1.112E+04	8.035E+03	4.678E+04	7.112E+03	1.467E+04	2.197E+06	1.353E+04	6.875E+05	1.193E+06	6.810E+05	1.257E+07	**1.004E+03**
F66	*AVG*	**1.375E+03**	3.824E+03	1.392E+04	1.784E+03	1.015E+04	9.703E+04	1.662E+04	3.198E+04	3.214E+04	2.686E+04	2.861E+05	1.429E+03
	SD	**1.979E+01**	8.557E+02	2.743E+04	5.198E+02	8.031E+03	6.739E+04	1.519E+04	2.499E+04	2.683E+04	2.591E+04	3.580E+05	3.575E+01
F67	*AVG*	**1.437E+03**	1.595E+03	1.575E+03	1.568E+03	1.609E+03	1.137E+04	1.804E+03	3.478E+04	2.899E+04	2.282E+04	4.080E+04	1.451E+03
	SD	**7.645E+00**	6.280E+01	1.816E+02	6.329E+01	2.297E+02	8.861E+03	2.986E+02	2.534E+04	1.735E+04	3.415E+04	3.319E+04	1.038E+01
F68	*AVG*	**1.518E+03**	1.835E+03	1.656E+03	1.723E+03	3.206E+03	2.6019E+04	2.054E+03	1.623E+04	2.411E+04	1.109E+04	5.919E+04	1.553E+03
	SD	**4.418E+00**	1.471E+02	1.943E+02	1.094E+02	2.841E+03	1.512E+04	9.221E+02	1.476E+04	1.449E+04	8.318E+03	4.098E+04	1.469E+01
F69	*AVG*	**2.060E+03**	2.084E+03	2.221E+03	2.113E+03	2.118E+03	2.462E+03	2.685E+03	2.749E+03	2.489E+03	2.525E+03	2.499E+03	2.081E+03
	SD	1.752E+02	1.685E+02	1.849E+02	1.688E+02	**1.580E+02**	2.885E+02	2.753E+02	2.793E+02	2.688E+02	2.917E+02	2.475E+02	1.856E+02
F70	*AVG*	1.824E+03	1.869E+03	1.925E+03	1.859E+03	**1.760E+03**	2.018E+03	2.218E+03	2.283E+03	2.155E+03	2.132E+03	2.077E+03	1.843E+03
	SD	7.587E+01	8.466E+01	8.469E+01	8.908E+01	**6.625E+01**	1.856E+02	1.712E+02	2.731E+02	1.809E+02	2.226E+02	1.237E+02	7.792E+01
F71	*AVG*	1.888E+03	2.098E+03	6.040E+03	2.634E+03	3.168E+04	1.578E+05	9.080E+03	2.623E+05	3.450E+05	2.614E+05	6.213E+05	**1.882E+03**
	SD	1.010E+02	1.543E+02	3.898E+03	1.065E+03	2.527E+04	2.030E+05	1.0418E+04	2.329E+05	3.270E+05	3.401E+05	3.735E+05	**2.211E+01**
F72	*AVG*	**1.914E+03**	2.127E+03	2.026E+03	2.027E+03	4.304E+03	3.715E+05	2.053E+03	1.767E+04	3.278E+04	1.348E+04	2.912E+05	1.926E+03
	SD	**2.875E+00**	1.237E+02	3.7955E+02	7.403E+01	2.966E+03	1.948E+05	6.999E+01	1.783E+04	1.970E+04	1.224E+04	3.449E+05	4.728E+00
F73	*AVG*	2.183E+03	2.191E+03	2.178E+03	2.221E+03	**2.092E+03**	2.389E+03	2.542E+03	2.526E+03	2.443E+03	2.360E+03	2.334E+03	2.179E+03

(*Continued on next page*)

Table 7. *Continued*

Function	Metric	DDRIME	LSHADE_cnEpSi	EPSDE	LSHADE	SADE	WLSSA	INFO	HGS	SMA	ALCPSO	IGWO	DFSMA
	SD	7.973E+01	9.342E+01	7.754E+01	1.002E+02	**6.828E+01**	1.236E+02	2.194E+02	2.342E+02	1.709E+02	1.922E+02	1.345E+02	8.848E+01
F74	*AVG*	2.353E+03	2.341E+03	2.341E+03	**2.335E+03**	2.341E+03	2.397E+03	2.439E+03	2.417E+03	2.401E+03	2.406E+03	2.397E+03	2.366E+03
	SD	1.201E+01	8.993E+00	**8.674E+00**	1.005E+01	1.130E+01	2.631E+01	3.579E+01	3.041E+01	2.047E+01	3.776E+01	2.512E+01	3.536E+01
F75	*AVG*	3.108E+03	2.708E+03	5.288E+03	2.471E+03	2.301E+03	2.300E+03	4.853E+03	4.883E+03	5.748E+03	4.789E+03	2.311E+03	**2.300E+03**
	SD	1.378E+03	8.514E+02	1.519E+03	6.447E+02	1.412E+00	1.028E+00	2.057E+03	1.401E+03	9.067E+02	1.799E+03	1.802E+00	**1.749E-04**
F76	*AVG*	2.701E+03	2.712E+03	2.695E+03	**2.685E+03**	2.691E+03	2.764E+03	2.829E+03	2.775E+03	2.738E+03	2.797E+03	2.770E+03	2.719E+03
	SD	1.062E+01	2.182E+01	1.200E+01	**1.049E+01**	1.144E+01	2.305E+01	5.403E+01	2.784E+01	2.838E+01	5.625E+01	3.059E+01	1.755E+01
F77	*AVG*	2.881E+03	2.885E+03	2.871E+03	**2.861E+03**	2.8677E+03	2.929E+03	2.994E+03	3.022E+03	2.923E+03	2.979E+03	2.939E+03	2.890E+03
	SD	1.333E+01	2.099E+01	**1.016E+01**	1.334E+01	1.698E+01	3.267E+01	4.877E+01	5.156E+01	2.538E+01	7.169E+01	2.591E+01	1.772E+01
F78	*AVG*	2.887E+03	2.897E+03	**2.878E+03**	2.891E+03	2.899E+03	2.901E+03	2.906E+03	2.890E+03	2.890E+03	2.901E+03	2.901E+03	2.886E+03
	SD	**1.108E+00**	1.658E+01	1.488E+00	1.009E+01	1.920E+01	1.859E+01	2.329E+01	1.295E+01	1.261E+01	1.871E+01	1.710E+01	1.399E+00
F79	*AVG*	4.173E+03	4.024E+03	3.803E+03	4.022E+03	3.954E+03	4.528E+03	6.037E+03	4.788E+03	4.514E+03	4.751E+03	4.794E+03	**3.663E+03**
	SD	2.706E+02	5.884E+02	**1.537E+02**	2.533E+02	5.862E+02	9.607E+02	8.376E+02	6.442E+02	2.062E+02	7.602E+02	3.088E+02	7.991E+02
F80	*AVG*	3.207E+03	3.232E+03	**3.201 + 03**	3.226E+03	3.227E+03	3.243E+03	3.256E+03	3.232E+03	3.213E+03	3.251E+03	3.238E+03	3.205E+03
	SD	5.046E+00	1.684E+01	**1.180E-04**	1.421E+01	1.047E+01	2.262E+01	2.270E+01	1.747E+01	1.234E+01	3.087E+01	1.533E+01	8.585E+00
F81	*AVG*	3.144E+03	3.154E+03	3.299E+03	3.167E+03	3.154E+03	3.209E+03	3.126E+03	3.201E+03	3.243E+03	3.231E+03	3.255E+03	**3.123E+03**
	SD	6.035E+01	6.109E+01	**2.509E+00**	7.005E+01	5.663E+01	3.075E+01	4.954E+01	4.334E+01	3.689E+01	6.315E+01	3.008E+01	3.667E+01
F82	*AVG*	3.422E+03	3.522E+03	3.388E+03	3.503E+03	**3.370E+03**	3.983E+03	4.079E+03	3.766E+03	3.740E+03	3.834E+03	3.797E+03	3.531E+03
	SD	7.112E+01	1.191E+02	9.787E+01	1.357E+02	**3.901E+01**	2.728E+02	2.782E+02	2.018E+02	1.549E+02	2.457E+02	1.488E+02	1.329E+02
F83	*AVG*	5.363E+03	5.904E+03	**3.244E+03**	5.389E+03	7.034E+03	1.804E+06	6.394E+03	7.678E+04	1.591E+04	1.632E+04	3.931E+06	5.339E+03
	SD	5.078E+02	5.171E+02	**4.478E+01**	3.216E+02	1.234E+03	1.203E+06	1.090E+03	1.254E+05	6.208E+03	1.458E+04	2.826E+06	2.355E+02

Table 8. Comparison average error rate values of the mentioned optimizers

Dataset	Metric	bSMA	bHGS	bHHO	bRUN	bIGWO	bDFSMA	bISMA	bAOA	bINFO	bGBO	bRIME	bDDRIME
Brain_Tumor2	*SD*	0	0	0	0.1725	0	0	0	0.1044	0	0	0.0866	0
	AVG	0	0	0	0.2033	0	0	0	0.0486	0	0	0.0393	0
DLBCL	*SD*	0	0	0	0.1450	0	0	0	0.0431	0	0	0	0
	AVG	0	0	0	0.1061	0	0	0	0.0130	0	0	0	0
IonosphereEW	*SD*	0.0203	0.0147	0.0204	0.0578	0.0147	0.0270	0.0120	0.0148	0.0181	**0.0090**	0.0138	**0.0090**
	AVG	0.0115	0.0113	0.0116	0.0630	0.0113	0.0113	0.0057	0.0114	0.0057	**0.0029**	0.0086	**0.0029**
Leukemia	*SD*	0	0	0	0.0902	0	0	0	0	0	0	0	0
	AVG	0	0	0	0.1113	0	0	0	0	0	0	0	0
Leukemia1	*SD*	0	0	0	0.0972	0	0	0	0	0	0	0	0
	AVG	0	0	0	0.1006	0	0	0	0	0	0	0	0
Leukemia2	*SD*	0	0	0	0.0736	0	0	0	0.0452	0	0	0	0
	AVG	0	0	0	0.0696	0	0	0	0.0143	0	0	0	0
Lung_Cancer	*SD*	0.0151	0.0151	0.0234	0.0556	0.0256	0	0.0151	0.0246	0.0206	0.0151	0.0253	0
	AVG	0.0048	0.0048	0.0145	0.0834	0.0198	0	0.0048	0.0153	0.0098	0.0048	0.0195	0
penglungEW	*SD*	0	0	0	0.0981	0	0	0	0	0	0	0.0395	0
	AVG	0	0	0	0.1220	0	0	0	0	0	0	0.0125	0
Prostate_Tumor	*SD*	0	0	0	0.1375	0.0316	0	0	0.0895	0.0632	0	0.0422	0
	AVG	0	0	0	0.1255	0.0100	0	0	0.0664	0.0200	0	0.0200	0
Tumors_11	*SD*	0.0298	0.0295	0.0388	0.0781	0.0938	0.0852	0.0228	0.0533	0.0855	0.0176	0.0404	**0.0166**
	AVG	0.0344	0.0226	0.0168	0.1088	0.1448	0.1503	0.0108	0.0429	0.1488	0.0056	0.0226	**0.0053**
SRBCT	*SD*	0	0	0	0.0499	0	0	0	0	0	0	0	0
	AVG	0	0	0	0.0236	0	0	0	0	0	0	0	0
Tumors_14	*SD*	0.0486	0.0466	**0.0407**	0.1019	0.0686	0.0471	0.0683	0.0603	0.0575	0.0749	0.0682	0.0478
	AVG	0.2668	0.2398	0.2178	0.3397	0.2595	0.2485	0.2352	0.2813	0.2700	0.2221	0.2779	**0.2034**
Rank-ARV		3.0000	2.2500	2.7500	11.7500	4.0833	2.7500	1.7500	7.0833	3.8333	1.4167	5.4167	**1.0000**
Rank		7	4	5	12	9	5	3	11	8	2	10	**1**

Table 9. The number of selected features gained by the mentioned optimizers

Dataset	Metric	bSMA	bHGS	bHHO	bRUN	bIGWO	bDFSMA	bISMA	bAOA	bINFO	bGBO	bRIME	bDDRIME
Brain_Tumor2	*SD*	167.5246	**1.1738**	28.6325	1224.6475	119.9474	18.3875	1.8529	1220.3752	309.3948	19.3563	633.9268	1.912
	AVG	213.6	2.6	22.6	3899.5	157.6	12.9	**2.1**	859.3	409.5	20	660.4	**2.1**
DLBCL	*SD*	73.6593	0.8312	3.8589	471.0054	99.396	3.1392	**0.3015**	179.5299	87.0888	4.1429	274.923	**0.3015**
	AVG	46.9091	2.0909	4.0909	2010.0909	110.8182	3.3636	**1.0909**	296	153.6364	3.8182	277.6364	**1.0909**
IonosphereEW	*SD*	2.675	2.2608	2.1187	3.4254	2.5927	1.6997	2.3664	3.4075	1.5239	4.0346	1.1738	**1.0541**
	AVG	5.6	5	5.6	12.2	6.5	5	4.6	10.5	5.9	7.5	8.6	**4**
Leukemia	*SD*	24.5423	0.48305	11.5224	883.9645	117.9814	8.9623	**0.31623**	386.639	155.826	6.9194	174.9694	**0.3162**
	AVG	35.9	1.7	13.1	2388.1	181.4	4.9	**1.1**	409.8	240.8	7.9	304.5	**1.1**
Leukemia1	*SD*	80.4958	0.7379	27.1008	679.095	172.2821	6.624	0.99443	218.4025	125.8987	7.3756	397.6104	**0.6325**
	AVG	78.3	2.1	25.3	2015	215.3	10.1	2.1	405.1	207.6	15.8	533	**1.8**
Leukemia2	*SD*	71.5138	**0.84327**	37.5868	1268.3562	113.8395	5.5538	2.0656	479.8327	108.2448	6.168	702.7966	1.0593
	AVG	73	2.6	34.9	3918.7	157.9	6.2	2.6	484.6	304.5	9.6	589.2	**1.7**
Lung_Cancer	*SD*	83.5852	28.649	39.2526	1600.2674	427.4939	140.6574	26.144	959.861	437.0897	186.5415	1033.5186	**18.0862**
	AVG	178.4	**21.9**	102.1	4231.1	568.8	124.5	25.2	1354.3	1002.1	152.2	1722.6	22
penglungEW	*SD*	6.0516	2.9136	3.9721	40.0616	11.2368	2.6013	4.2479	24.9464	8.5667	1.7127	14.5388	**1.6499**
	AVG	9.8	4.4	6	98.6	17.4	4.1	3.4	33.9	13.5	3.6	21.4	**2.5**
Prostate_Tumor	*SD*	146.0883	3.2677	41.2797	1122.589	672.7783	130.0938	7.3401	1054.9111	379.1521	48.8262	1081.2041	**1.3499**
	AVG	249	4.7	49.7	3402.2	569.8	69.8	5.9	1251.5	772.5	70	1559.5	**2.4**
Tumors_11	*SD*	137.6301	227.3892	185.3885	1935.5878	**0**	**0**	254.7536	1895.4958	**0**	226.26	854.2834	122.2813
	AVG	410.5	275.5	499	4364.3	**0**	**0**	418.6	2857.4	**0**	505.7	2687.5	247.4
SRBCT	*SD*	18.2343	2.044	7.0048	312.0504	57.6469	4.6774	2.5927	114.6642	32.0293	6.7074	136.5279	**0.9661**
	AVG	26.6	5.2	14.8	706.1	73.5	7.9	4.5	196.9	81.1	10.1	155.9	**2.6**
Tumors_14	*SD*	1353.4534	**357.3082**	728.9322	1008.8851	1730.5731	614.6823	1418.5611	1620.272	802.011	1590.8417	1378.4948	861.4415
	AVG	1193.9	**762.6**	1607.9	6005.6	3210.6	1964.9	1162	6706.2	4130.3	2829.8	5291.5	1457.5
Rank-ARV		6.5000	2.7500	5.6667	11.9167	7.5000	4.0000	2.3333	10.7500	8.0000	5.8333	10.3333	**1.5833**
Rank		7	3	5	12	8	4	2	11	9	6	10	**1**

Table 10. The best fitness values of the mentioned swarm intelligent optimizers

Dataset	Metric	bSMA	bHGS	bHHO	bRUN	bIGWO	bDFSMA	bISMA	bAOA	bINFO	bGBO	bRIME	bDDRIME
Brain_Tumor2	*SD*	8.08E-04	**5.66E-06**	1.38E-04	8.02E-02	5.79E-04	8.87E-05	8.94E-06	1.04E-01	1.49E-03	9.34E-05	8.09E-02	9.22E-06
	AVG	1.03E-03	1.25E-05	1.09E-04	4.55E-02	7.60E-04	6.22E-05	**1.01E-05**	5.03E-02	1.98E-03	9.65E-05	4.05E-02	**1.01E-05**
DLBCL	*SD*	6.73E-04	7.60E-06	3.53E-05	2.15E-03	9.09E-04	2.87E-05	**2.76E-06**	4.09E-02	7.96E-04	3.79E-05	2.51E-03	**2.76E-06**
	AVG	4.29E-04	1.91E-05	3.74E-05	7.09E-03	1.01E-03	3.08E-05	**9.97E-06**	1.50E-02	1.40E-03	3.49E-05	2.54E-03	**9.97E-06**
IonosphereEW	*SD*	1.87E-02	1.30E-02	1.91E-02	2.10E-02	1.35E-02	2.50E-02	1.07E-02	1.27E-02	1.68E-02	**8.30E-03**	1.30E-02	8.72E-03
	AVG	1.92E-02	1.81E-02	1.93E-02	2.60E-02	2.03E-02	1.81E-02	1.22E-02	2.63E-02	1.41E-02	1.37E-02	2.08E-02	**8.60E-03**
Leukemia	*SD*	1.72E-04	3.39E-06	8.08E-05	2.78E-03	8.27E-04	6.28E-05	**2.22E-06**	2.71E-03	1.09E-03	4.85E-05	1.23E-03	**2.22E-06**
	AVG	2.52E-04	1.19E-05	9.19E-05	7.32E-03	1.27E-03	3.44E-05	**7.71E-06**	2.87E-03	1.69E-03	5.54E-05	2.14E-03	**7.71E-06**
Leukemia1	*SD*	7.56E-04	6.93E-06	2.54E-04	2.74E-03	1.62E-03	6.22E-05	9.33E-06	2.05E-03	1.18E-03	6.92E-05	3.73E-03	**5.94E-06**
	AVG	7.35E-04	1.97E-05	2.37E-04	9.26E-03	2.02E-03	9.48E-05	1.97E-05	3.80E-03	1.95E-03	1.48E-04	5.00E-03	**1.69E-05**
Leukemia2	*SD*	3.19E-04	**3.76E-06**	1.67E-04	2.87E-03	5.07E-04	2.47E-05	9.20E-06	4.25E-02	4.82E-04	2.75E-05	3.13E-03	4.72E-06
	AVG	3.25E-04	1.16E-05	1.55E-04	6.76E-03	7.03E-04	2.76E-05	1.16E-05	1.57E-02	1.36E-03	4.28E-05	2.62E-03	**7.57E-06**
Lung_Cancer	*SD*	1.42E-02	1.43E-02	2.22E-02	2.99E-02	2.54E-02	5.58E-04	1.43E-02	2.32E-02	1.93E-02	1.50E-02	2.63E-02	**7.18E-05**
	AVG	5.23E-03	4.61E-03	1.42E-02	2.11E-02	2.11E-02	4.94E-04	4.62E-03	1.99E-02	1.33E-02	5.13E-03	2.54E-02	**8.73E-05**
penglungEW	*SD*	9.31E-04	4.48E-04	6.11E-04	2.93E-03	1.73E-03	4.00E-04	6.54E-04	3.84E-03	1.32E-03	2.63E-04	3.78E-02	**2.54E-04**
	AVG	1.51E-03	6.77E-04	9.23E-04	7.06E-03	2.68E-03	6.31E-04	5.23E-04	5.22E-03	2.08E-03	5.54E-04	1.52E-02	**3.85E-04**
Prostate_Tumor	*SD*	6.95E-04	1.55E-05	1.96E-04	5.92E-02	3.15E-02	6.19E-04	3.49E-05	8.56E-02	6.10E-02	2.32E-04	4.07E-02	**6.42E-06**
	AVG	1.18E-03	2.24E-05	2.36E-04	2.95E-02	1.22E-02	3.32E-04	2.81E-05	6.90E-02	2.27E-02	3.33E-04	2.64E-02	**1.14E-05**
Tumors_11	*SD*	2.80E-02	2.86E-02	3.68E-02	2.99E-02	8.91E-02	8.10E-02	2.15E-02	5.14E-02	8.13E-02	1.70E-02	3.82E-02	**1.61E-02**
	AVG	3.43E-02	2.25E-02	1.79E-02	4.31E-02	1.88E-01	1.93E-01	1.19E-02	5.22E-02	1.91E-01	7.30E-03	3.22E-02	**5.99E-03**
SRBCT	*SD*	3.95E-04	4.43E-05	1.52E-04	2.05E-03	1.25E-03	1.01E-04	5.62E-05	2.48E-03	6.94E-04	1.45E-04	2.96E-03	**2.09E-05**
	AVG	5.76E-04	1.13E-04	3.21E-04	6.07E-03	1.59E-03	1.71E-04	9.75E-05	4.27E-03	1.76E-03	2.19E-04	3.38E-03	**5.63E-05**
Tumors_14	*SD*	4.68E-02	4.48E-02	**3.90E-02**	7.86E-02	6.53E-02	4.50E-02	6.46E-02	5.39E-02	5.53E-02	6.77E-02	6.50E-02	4.52E-02
	AVG	2.57E-01	2.30E-01	2.12E-01	2.79E-01	2.57E-01	2.43E-01	2.27E-01	2.90E-01	2.70E-01	2.20E-01	2.82E-01	**1.98E-01**
Rank-ARV		7.0000	3.4167	5.6667	10.8333	8.4167	4.8333	2.2500	11.0000	8.4167	4.3333	10.1667	**1.0000**
Rank		7	3	6	11	8	5	2	12	8	4	10	**1**

Table 11. Time cost of the mentioned swarm intelligent optimizers

Dataset	Metric	bSMA	bHGS	bHHO	bRUN	bIGWO	bDFSMA	bISMA	bAOA	bINFO	bGBO	bDDRIME	bRIME
Brain_Tumor2	*SD*	1.3403	1.8348	1.3478	1.9825	0.4576	0.3714	3.1385	**0.2978**	0.7971	0.3276	1.1381	0.7240
	AVG	78.4246	36.4100	42.6648	48.6295	35.7996	36.1942	130.3329	19.5642	16.6014	**15.2564**	46.4069	25.2528
DLBCL	*SD*	0.5091	0.3277	0.4037	0.5226	0.2902	0.4208	5.4182	0.2673	0.2643	**0.2401**	1.3182	0.2785
	AVG	19.1494	**13.6429**	22.6195	31.9593	22.5244	32.0288	162.0022	18.1771	15.2069	14.8058	40.5406	16.5376
IonosphereEW	*SD*	**0.0861**	0.1206	0.0969	0.1913	0.1788	0.1655	0.4618	0.1996	0.1313	0.2165	0.5561	0.1643
	AVG	**3.2504**	3.2966	4.9885	5.2427	4.3286	8.2602	32.5564	3.7628	5.3134	6.9608	14.6240	5.7820
Leukemia	*SD*	0.3684	0.3751	0.7065	1.2193	**0.3176**	0.5437	7.7030	0.5056	0.7044	0.3637	2.8288	0.6263
	AVG	46.1571	**16.1108**	26.2869	36.9165	26.2042	38.1702	208.1876	32.6637	23.3892	26.6399	56.2352	26.8119
Leukemia1	*SD*	0.2506	**0.1273**	0.2657	0.4999	0.2078	0.2169	2.7685	0.1785	0.5130	0.2938	0.7970	0.1724
	AVG	13.8993	**7.8565**	14.5854	17.8542	14.2666	19.0139	79.9625	16.4997	12.9091	12.5995	32.9981	14.1796
Leukemia2	*SD*	0.8435	0.4211	0.6075	0.9468	0.4755	0.5417	5.7126	0.3665	0.3454	0.7215	0.8811	**0.3228**
	AVG	58.1680	**21.4835**	37.1911	52.6570	37.1116	50.9559	178.9998	31.9589	23.9059	22.3900	60.8832	28.5735
Lung_Cancer	*SD*	**1.1320**	1.4720	5.5550	6.8422	3.6912	3.0071	57.9613	1.5738	1.5080	2.7789	4.1551	3.4165
	AVG	107.1421	**50.4855**	118.3708	191.6859	162.1882	189.9620	651.7133	156.6131	85.9377	61.5586	236.6337	171.6769
penglungEW	*SD*	0.1779	**0.1262**	0.2380	0.3269	0.1551	0.3705	1.0659	0.4525	0.2659	0.1866	0.3399	0.1429
	AVG	8.2429	5.4955	9.1164	8.9718	6.7230	10.0987	39.6212	7.2410	8.7390	7.7502	15.2131	**5.3580**
Prostate_Tumor	*SD*	0.5373	0.6387	1.9834	1.1432	0.7449	0.6092	5.1336	0.3039	1.2332	0.7849	1.4597	**0.1797**
	AVG	37.7940	**20.6607**	50.6721	76.3293	54.2194	84.5999	198.1384	42.6779	33.4345	30.6583	76.6733	38.1298
Tumors_11	*SD*	8.7807	9.5911	5.9860	9.8088	7.5266	6.9202	13.7317	2.4238	2.9252	1.6891	3.6304	**0.6595**
	AVG	118.7592	153.4658	218.0242	223.1487	303.1839	360.5019	381.3650	100.7618	179.8759	**55.7010**	151.8555	106.2055
SRBCT	*SD*	0.1078	**0.0902**	0.2202	0.1922	0.1830	0.1009	0.9793	0.1171	0.1338	0.1211	0.2042	0.1495
	AVG	6.7045	**4.4430**	8.4302	16.7718	14.5440	12.0865	36.2600	6.1685	5.3066	5.2941	13.8056	5.6907
Tumors_14	*SD*	**11.8632**	12.1080	18.6170	33.2921	17.6725	39.3633	94.9965	19.9882	16.4329	16.1325	32.9260	21.3199
	AVG	196.0070	**71.6646**	169.5153	285.5003	218.6937	256.0372	700.0649	180.1616	134.7022	110.1989	251.1285	158.4546
Rank-ARV		5.8333	**1.7500**	6.5000	9.1667	6.5833	9.1667	11.0833	5.7500	4.4167	3.2500	9.2500	5.1667
Rank		6	**1**	7	9	8	9	12	5	3	2	11	4

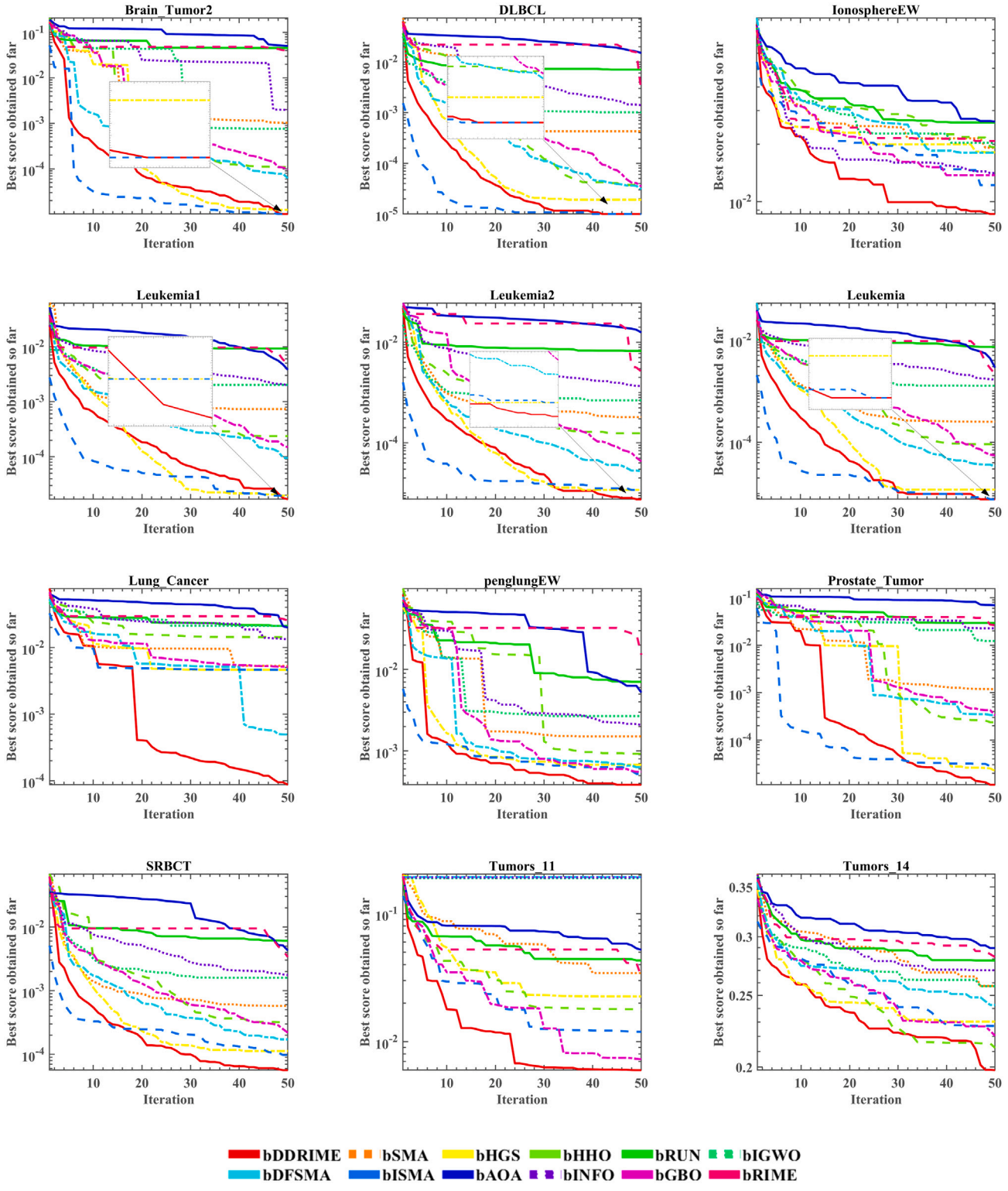

Figure 3. Curves of bDDRIME and mentioned binary methods on public datasets

The accuracy *(ACC)* rate is an important indicator of classification performance, which is expressed as the percentage of correctly classified instances as Equation 1.

$$ACC = \frac{TP+TN}{TP+FP+FN+TN} \quad \text{(Equation 1)}$$

where TP represents the number of correctly classified positive samples. TN denotes the correctly identified negative samples. FN means the positive samples that are incorrectly labeled as negative. FP indicates negative samples that are mistakenly classified as positive.

Precision represents the percentage of the positive samples predicted to be positive samples as Equation 2.

$$Precision = \frac{TP}{TP+FP} \quad \text{(Equation 2)}$$

Specificity measures the ability of a binary classification model to identify normal instances as Equation 3.

$$Specificity = \frac{TN}{FP+TN} \quad \text{(Equation 3)}$$

MCC evaluates the classifier model's performance. It incorporates all four criteria (*TP, TN, FP, FN*) and may offer a more accurate assessment than percentages as Equation 4.

$$MCC = \frac{TP \times TN - FP \times FN}{\sqrt{(TP+FP) \times (TP+FN) \times (TN+FP) \times (TN+FN)}} \quad \text{(Equation 4)}$$

Recall represents the ratio of actual positive samples in the predicted positives to the total positive samples in the entire dataset as Equation 5.

$$Recall = \frac{TP}{TP+FN} \quad \text{(Equation 5)}$$

F-measure is a metric that combines precision and recall into a weighted average as Equation 6.

$$F - measure = 2 * \frac{Precision * \text{Recall}}{Precision+\text{Recall}} \quad \text{(Equation 6)}$$

Then, we apply bDDRIME_KNN along with some well-known classifiers, including bDDRIME_KELM, bDDRIME_FKNN, bDDRIME_MLP, and bDDRIME_SVM. Figure 4 illustrates the time, *ACC*, *precision*, *specificity*, *MCC*, and *F-measure*. The graph shows that DDRIME achieves the fastest convergence time, *ACC*, *precision*, *specificity*, *MCC*, and *F-measure* compared to the other classifiers. This further substantiates the effectiveness and reliability of the bDDRIME_KNN model's capability.

Furthermore, bDDRIME_KNN compares against bSMA_KNN, bHGS_KNN, bHHO_KNN, bRUN_KNN, bIGWO_KNN, bDFSMA_KNN, bISMA_KNN, bAOA_KNN, bINFO_KNN, bGBO_KNN, and bRIME_KNN for feature selection on the AECOPD dataset. Figure 5 showcases the time cost, *ACC*, *specificity*, *precision*, *MCC*, and *F-measure* of these methods. The time cost of bISMA_KNN is the most, and the proposed method takes the second most time. The proposed bDDRIME_KNN model ranks first on *ACC*, *specificity*, *precision*, *MCC*, and *F-measure*, which demonstrates excellent performance for feature selection on the AECOPD dataset.

In summary, the two mechanisms proposed in this study have a significant influence on enhancing RIME's optimization performance. The introduced bDDRIME_KNN model effectively identifies the optimal subset on the AECOPD dataset. This confirms the practicality and outstanding optimization capabilities of the proposed DDRIME algorithm.

Figure 6 shows the fitness value obtained by bSMA_KNN, bHGS_KNN, bHHO_KNN, bRUN_KNN, bIGWO_KNN, bDFSMA_KNN, bISMA_KNN, bAOA_KNN, bINFO_KNN, bGBO_KNN, and bRIME_KNN on the AECOPD dataset. It can be seen that the proposed bDDRIME_KNN model reaches the best fitness after several iterations, which demonstrates the excellent performance for feature selection on the AECOPD dataset.

All in all, to further help physicians analyze the classification results, we analyzed the features specifically in the 10-fold CV experimental results. The features selected in each experiment are presented in Figure 7. It is seen from Figure 7 that the features with the highest selection frequency are C1, C3, C7, and C8. Further analysis shows that the features of C1, C3, C7, and C8 are the most crucial for the dataset. Therefore, bDDRIME_KNN provides accurate classification results for doctors to find useful subsets in the AECOPD data.

Discussion

We included a detailed analysis of the results, explaining the significance of the findings from the DDRIME algorithm and its application in the bDDRIME_KNN model. We have discussed how the improved search ability and feature selection performance of DDRIME contribute to the enhanced predictive accuracy for AECOPD patients on IMV. We have provided justifications for our results by comparing them with existing methods and algorithms. We have addressed the scenarios where our model outperforms others and also the areas where it aligns with current standards, offering possible explanations for these observations. We elaborated on the clinical implications of our findings, discussing how the DDRIME algorithm could potentially impact the management and prognosis of AECOPD patients requiring IMV. From Figure 7, it

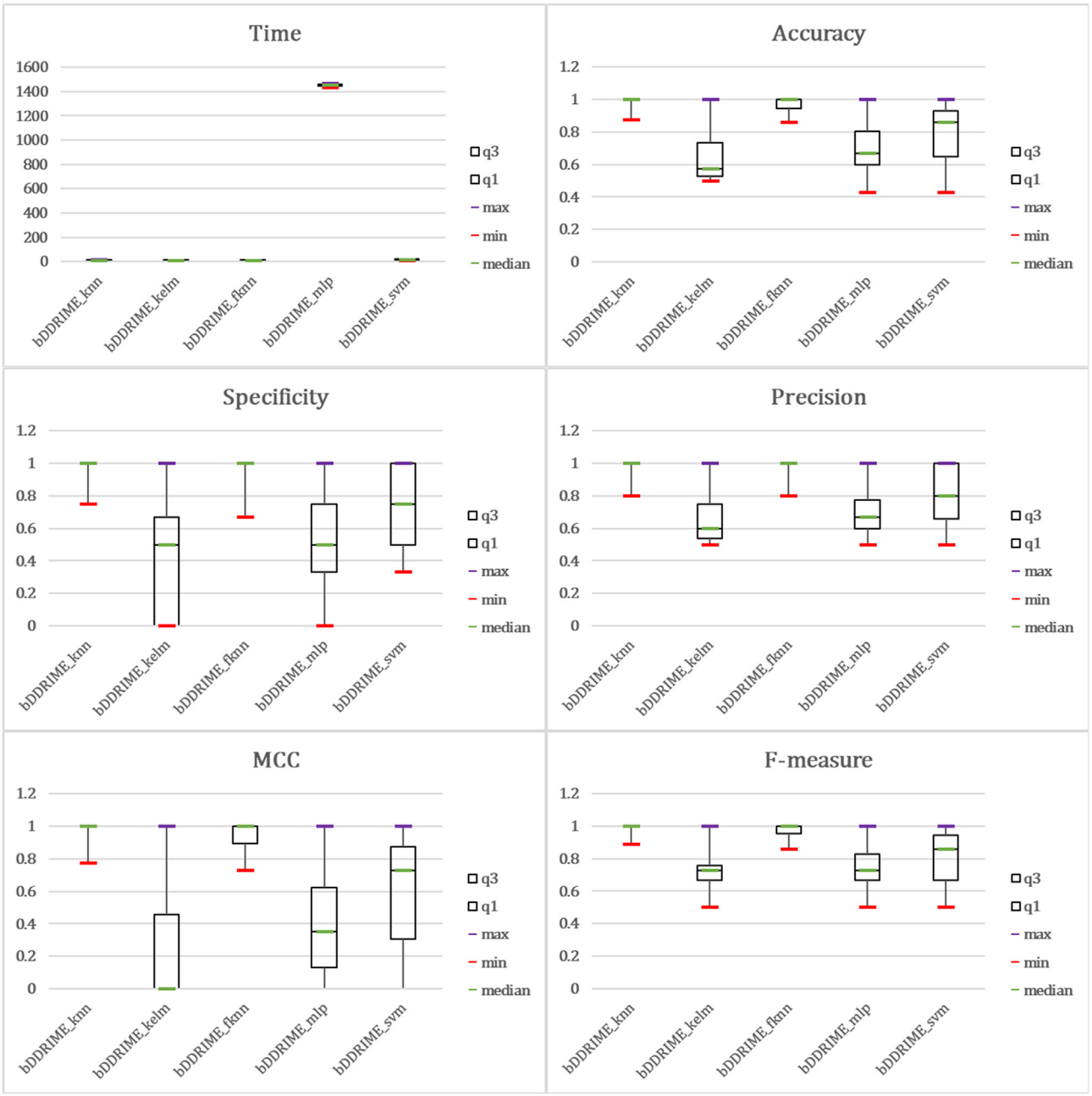

Figure 4. Boxplot results for five DDRIME-based classifiers on the AECOPD dataset

can be seen that in the experimental results of feature selection using the proposed DDRIME algorithm in the AECOPD dataset, the most frequently selected features are C7 (pectoral muscle area [PMA]), C8 (D-dimer [D-D]), C1 (fungal infection [FI]), and C3 (chronic heart failure [CHF]). There is the detailed description of the selected features. D-D is a product of fibrin degradation, and it is commonly used to exclude venous thromboembolism,[57] but it is also elevated in the elderly, tumors, surgery, and infections.[58] In addition, D-D is considered an indicator for the evaluation of suspected pulmonary embolism,[59] and some studies have shown that patients with pulmonary embolism combined with AECOPD have higher D-D than AECOPD and higher mortality.[60] A retrospective study by Bai et al. confirmed that D-D is an independent risk factor for admission to the intensive care unit in patients with AECOPD.[61] A retrospective study by Zhang et al. found that D-D improved the sensitivity and specificity of predicting the probability of admission to the ICU in AECOPD.[62] Chen et al. found that D-D was significantly higher in patients with AECOPD than in COPD patients and healthy individuals.[63] Husebø et al. studied the prognostic predictive effect of coagulation indicators in COPD patients and showed that mortality was higher in COPD patients with high D-D (hazard ratios [HR]: 1.60

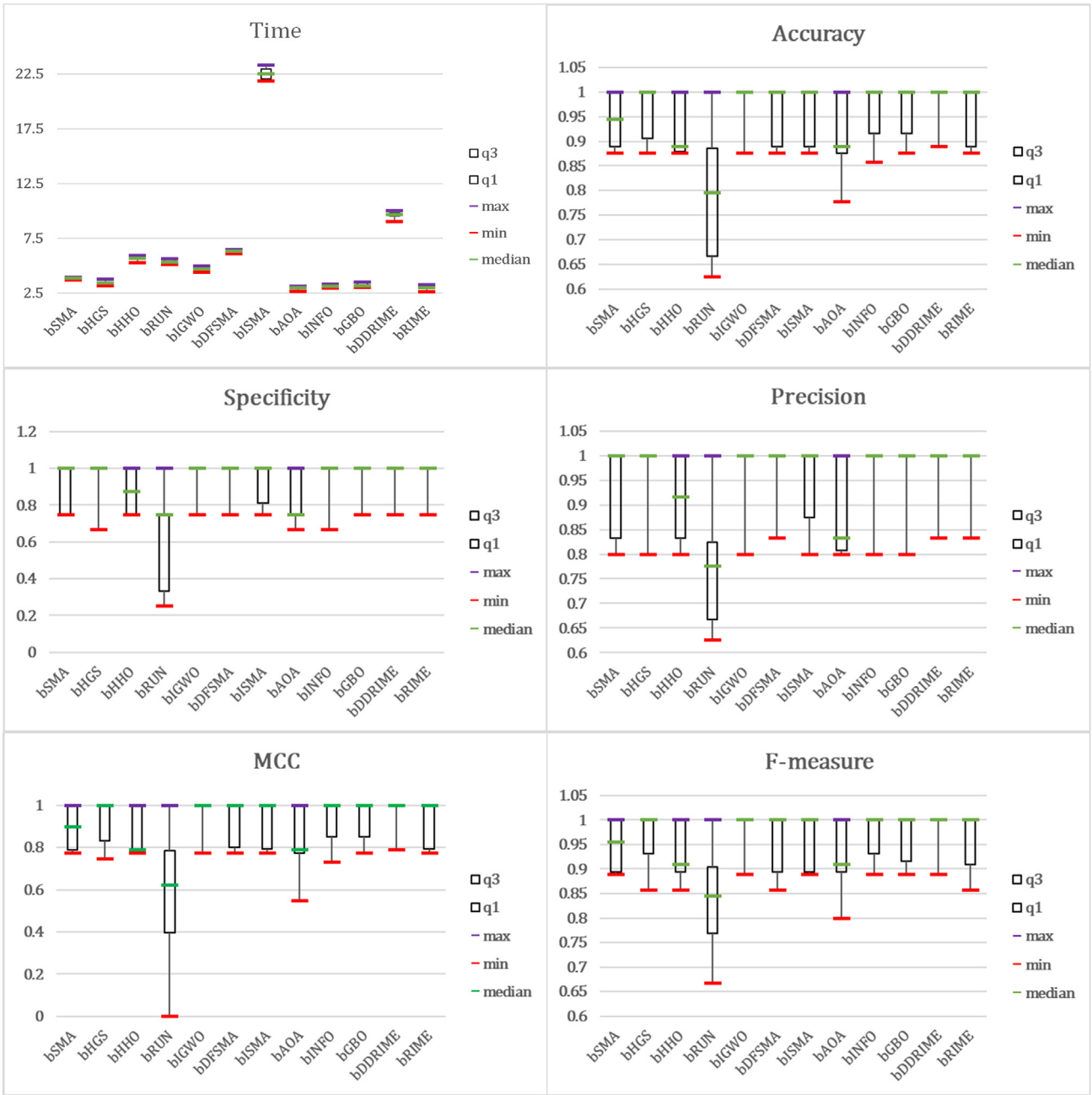

Figure 5. Boxplot results of 12 methods in six metrics on the AECOPD dataset

(1.24–2.05), $p < 0.001$) and that D-D was higher in AECOPD patients than in stable patients.[64] Fruchter et al. studied 61 patients with AECOPD and found that D-D >1.52 mg/L had higher sensitivity and specificity (100%) for predicting short-term mortality and higher long-term mortality than patients with less than 1.52 mg/L.[65] Hu et al. used a multifactorial logistic retrospective analysis and found that D-D was higher in patients with in-hospital death from AECOPD (2,244.9 ± 2,310.7) than in survivors (768.2 ± 1,078.4) and that D-D was an independent risk factor for predicting in-hospital death from AECOPD (95% confidence interval [CI] 1.05–3.65, $p < 0.05$).[66] Our study is similar to theirs, and this study found that high D-D will lead to poor prognosis in patients with IMV in AECOPD ($p < 0.05$); therefore, we need to pay prompt attention to the D-D level of patients after admission.

Pulmonary aspergillosis and pulmonary cryptococcosis are common fungal infectious diseases of the lung.[67,68] Patients with COPD are more susceptible to pulmonary fungal disease due to changes in lung structure, immunosuppression from hormone use, and frequent

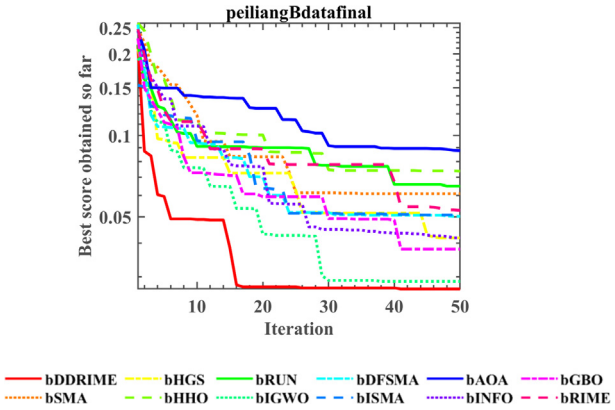

Figure 6. The fitness obtained by involved methods on the AECOPD dataset

antibiotic use.[69] A 1-year study by Bafadhel et al. found that aspergillus fumigatus infection was associated with reduced lung function in patients with COPD, with a significantly lower proportion of positive sputum filamentous fungal cultures in the control group.[70] Tanveer et al. showed by multifactorial logistic regression analysis that patients with AECOPD combined with pulmonary aspergillosis had a higher probability of cardiovascular events and neoplasms, and a higher mortality rate.[71] One study showed that among patients with COPD, Aspergillus definitive patients were more likely to develop aspergillosis.[72] In addition, Pneumocystis carinii colonization is also seen in COPD patients.[73] It has been demonstrated that elevated blood inflammatory markers (including tumor necrosis factor alpha, interleukin [IL]-6, and IL-8) and elevated matrix metalloproteinases (MMP-12) in AECOPD patients with Pneumocystis carinii infection damage the airways and lung parenchyma,[73,74] and a study by Morris et al. showed that MMP-12 values in the sputum of patients with Yersinia pseudomonas colonization (205.7 pg/mL) were significantly higher than in normal patients (47.7 pg/mL).[74] 90% of AECOPD exacerbations were caused by pathogens, with Chlamydia pneumoniae detected in 50% of patients.[75] In this study, the prognosis of AECOPD patients with fungal infections was found to be worse ($p < 0.05$); therefore, FI is an important predictor of prognosis for patients with AECOPD, and it is important to keep an eye on patients' infections for early detection and treatment.

CHF is a clinical syndrome of persistent slow manifestation of dyspnea, bilateral lower extremity edema, and jugular venous irritation based on pre-existing heart disease.[1] COPD and heart failure are often present together in many patients, and COPD patients with cardiac insufficiency are more likely to have an increased risk of death after discharge from the hospital.[76] Some studies confirm that markers of heart failure predict the prognosis of patients with AECOPD.[77,78] Tinè et al. found higher post-discharge mortality in patients with AECOPD combined with heart failure than in patients with AECOPD in their study's discharge follow-up (95% CI 1.4–3.1; $p = 0.002$).[79] Peng et al. concluded that chronic pulmonary heart disease was an independent risk factor for in-hospital mortality in patients with AECOPD by multifactorial regression analysis.[80] Curkendall et al. found a higher risk of death in COPD patients with comorbid cardiovascular disease, with higher hospitalization rates for CHF among different cardiovascular diseases.[81] A retrospective study by Cao et al. included 384 patients with AECOPD and concluded that in-hospital deaths were more common in patients with combined heart failure (50.0%) than in survivors (15.9%), and univariate and multivariate logistic regression analysis revealed that combined CHF was an independent risk factor for in-hospital mortality (odds ratio [OR] = 7.63, 95% CI: 2.27–25.64, $p = 0.001$).[82] In this study, AECOPD combined with chronic heart failure was statistically significant in the failure and success groups of IMV ($p = 0.024$). In summary, CHF is an important predictor of AECOPD prognosis. It is necessary to actively monitor the patient's cardiac function indicators and improve cardiac function.

Sarcopenia is a progressive systemic skeletal muscle disease with reduced muscle strength and mass leading to falls, fractures, and even death.[83] Sarcopenia is a common complication in COPD patients, and a meta-analysis by Elizabeth Benz et al. first evaluated the prevalence of sarcopenia in COPD patients at 21.6%, with high variability across settings.[84] The quality of skeletal muscle is an important indicator to assess the prognosis of COPD patients; with smaller PMAs, COPD patients have more severe obstruction of expiratory airflow and impaired motility.[85] McDonald et al. confirmed by examining COPD-related traits (FEV1/FVC, FEV1pred %, body mass index, etc.) that PMA (95% CI: 4.2–12.4, $p < 0.001$) was more significantly associated with COPD severity than BMI (95% CI: −12.2–0.4, $p = 0.03$), but the prognostic prediction of PMA on COPD progression remains to be studied.[86] A study by Mason et al. found that the development of AECOPD was associated with a loss of the pectoral muscle area.[87] A multivariate regression model test by Wilson et al. found that higher PMA reduced mortality in COPD and that the utility of PMA was higher than that of low bone mineral density.[88] In this study, PMA was significantly reduced in the failed IMV group compared to the successful group ($p < 0.05$). In conclusion, PMA is a valid prognostic predictor of AECOPD.

Our experiments and comparative analysis demonstrated that DDRIME, the enhanced version of RIME, outperformed the original algorithm and other MAs on various benchmark functions and real-world datasets. This confirms the effectiveness of our enhancement approach. It is identified that by incorporating a dispersed foraging mechanism and a differential crossover operator into RIME, we could

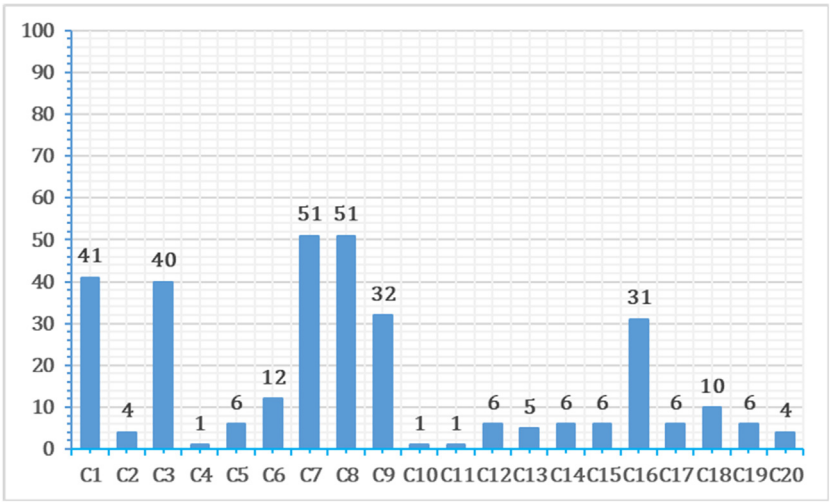

Figure 7. The number of selected features by bDDRIME_KNN on the AECOPD dataset

significantly improve its search capabilities. These enhancements are designed to boost exploration and avoid local optima, thereby enhancing the overall performance of the algorithm. By periodically dispersing the search agents, DDRIME can effectively avoid being trapped in local optima and enhance the diversity of the population, leading to a more comprehensive search. The differential crossover in DDRIME not only ensures that the new solutions are different from their parents but also maintains the balance between exploration and exploitation. This operator helps in refining the solutions obtained from the dispersed foraging mechanism, further improving the feature selection process.

In summary, the DDRIME algorithm specifically addresses the feature selection challenges of the original RIME by incorporating a nature-inspired dispersed foraging mechanism and a robust differential crossover operator. These enhancements work synergistically to improve the exploration and exploitation capabilities of the algorithm, leading to more effective feature selection.

Conclusions and future work

This article starts with an introduction to COPD and AECOPD, followed by the current medical applications of machine learning, and also details the data sources and related statistical methods. To effectively settle the issue of diagnosing medical conditions, an MA is employed to feature selection of interest. Among the various methods, this paper proposes a wrapper feature selection method using the DDRIME (dispersed foraging and differential evolution-based RIME) algorithm. This method initially uses DDRIME to find the optimal solution by minimizing the objective fitness function. The DDRIME algorithm is an enhancement of the RIME algorithm, incorporating dispersed foraging and differential crossover operators. These enhancements boost the agents' exploration of the search space, greatly increasing the chances of finding the optimal solution for 83 benchmark optimization problems. Thus, this demonstrates the strong competitiveness of the DDRIME algorithm in solving optimization cases. The results show that the aforementioned enhanced strategies effectively help search agents escape local optima and boost the population's exploration capability. Finally, comparative experiments with other MAs and classifiers have shown that the bDDRIME-KNN model demonstrates consistent performance and strengths in terms of *ACC*, specificity, precision, *MCC*, and F-measure metrics.

In the future, we will focus on utilizing DDRIME to optimize various fields like engineering, energy, neural network architectures, and clustering. Additionally, we will continue to refine DDRIME to better address the unique characteristics of different optimization problems. DDRIME can be integrated into existing optimization platforms and software tools used in various engineering fields, educational and research programs, and industry collaboration. Finally, we will examine the combined effects of neural networks with MAs for medical diagnosis.

Limitations of the study

While our study has achieved promising results, it is not without limitations. Firstly, the performance of DDRIME is evaluated primarily through computational experiments, and, thus, its application in real-world scenarios within AECOPD requires further validation. Secondly, the algorithm's parameters are tuned based on the benchmark functions, and their optimal values may vary when applied to different types of problems or datasets. Additionally, the computational cost of the DDRIME is relatively high, which could be a concern for large-scale applications. Addressing these limitations will be crucial for enhancing the algorithm's applicability and efficiency.

RESOURCE AVAILABILITY

Lead contact

Further requests for information should be directed and will be handled by the lead contact, Huiling Chen, email: chenhuiling.jlu@gmail.com.

Materials availability

This study did not generate new materials.

Data and code availability

- The dataset that informed or guided this study is available online, and data reported in this paper will be shared by the lead contact upon request.
- All original code generated as part of this study has been deposited at the website https://aliasgharheidari.com/ or at Zenodo and is publicly available as of the date of publication. A link to code and DOIs is listed in the key resources table.
- Any additional information for reanalyzing this work is available from the lead contact upon request.

ACKNOWLEDGMENTS

This study was supported by the Scientific Research Fund of Zhejiang Provincial Education Department (no. Y202353056).

AUTHOR CONTRIBUTIONS

H.C., P.W., and S.Y. contributed equally to the study conception and design.

H.C.: Writing - Original Draft, Conceptualization, Design, Experiment Design, Software.

P.W.: Writing - Original Draft, Conceptualization, Design, Experiment Design, Software.

S.Y.: Writing - Original Draft, Conceptualization, Design, Experiment Design, Software.

Y.F.: Experiment Execution, Data Collection, Data Analysis, Writing - Original Draft, Software.

Y.L.: Experiment Execution, Data Collection, Data Analysis, Writing - Original Draft, Software.

C.Z.: Data Collection, Data Analysis, Writing - Original Draft, Software.

A.A.H.: Writing - Original Draft, Writing - Critical Revision, Software.

L.L.: Writing - Original Draft, Writing - Critical Revision, Software.

S.Y.: Writing - Original Draft, Writing - Critical Revision, Experiment Design, Software.

All authors: Review & Editing, Approval of the Final Manuscript.

DECLARATION OF INTERESTS

The authors declare no competing interests.

STAR★METHODS

Detailed methods are provided in the online version of this paper and include the following:

- KEY RESOURCES TABLE
- METHOD DETAILS
  - RIME optimization
  - The initializing of Rime clusters
  - Soft-rime search
  - Hard-rime search
  - Positive greedy selection
  - KNN model
  - The dispersed foraging strategy
  - The differential crossover operator
  - Proposed methodology
- QUANTIFICATION AND STATISTICAL ANALYSIS

SUPPLEMENTAL INFORMATION

Supplemental information can be found online at https://doi.org/10.1016/j.isci.2024.111230.

Received: July 26, 2024
Revised: September 16, 2024
Accepted: October 21, 2024
Published: October 23, 2024

REFERENCES

1. McDonagh, T.A., Metra, M., Adamo, M., Gardner, R.S., Baumbach, A., Böhm, M., Burri, H., Butler, J., Čelutkienė, J., Chioncel, O., et al. (2021). 2021 ESC Guidelines for the diagnosis and treatment of acute and chronic heart failure. Eur. Heart J. *42*, 3599–3726.
2. Klinger, J.R., Wu, B., Morland, K., Classi, P., Fiano, R., and Grabich, S. (2023). Burden of pulmonary hypertension due to chronic obstructive pulmonary disease: Analysis of exacerbations and healthcare resource utilization in the United States. Respir. Med. *219*, 107412.
3. Vogelmeier, C.F., Criner, G.J., Martinez, F.J., Anzueto, A., Barnes, P.J., Bourbeau, J., Celli, B.R., Chen, R., Decramer, M., Fabbri, L.M., et al. (2017). Global Strategy for the Diagnosis, Management, and Prevention of Chronic Obstructive Lung Disease 2017 Report. GOLD Executive Summary. Am. J. Respir. Crit. Care Med. *195*, 557–582.
4. Hu, J., Gui, W., Heidari, A.A., Cai, Z., Liang, G., Chen, H., and Pan, Z. (2022). Dispersed foraging slime mould algorithm: Continuous and binary variants for global optimization and wrapper-based feature selection. Knowl. Base Syst. *237*, 107761.
5. Rabe, K.F., and Watz, H. (2017). Chronic obstructive pulmonary disease. Lancet *389*, 1931–1940.
6. Osadnik, C.R., Tee, V.S., Carson-Chahhoud, K.V., Picot, J., Wedzicha, J.A., and Smith, B.J. (2017). Non-invasive ventilation for the management of acute hypercapnic respiratory failure due to exacerbation of chronic obstructive pulmonary disease. Cochrane Database Syst. Rev. *2017*, Cd004104.
7. Marchioni, A., Tonelli, R., Fantini, R., Tabbì, L., Castaniere, I., Livrieri, F., Bedogni, S., Ruggieri, V., Pisani, L., Nava, S., and Clini, E. (2019). Respiratory Mechanics and Diaphragmatic Dysfunction in COPD Patients Who Failed Non-Invasive Mechanical Ventilation. Int. J. Chron. Obstruct. Pulmon. Dis. *14*, 2575–2585.
8. Lindenauer, P.K., Stefan, M.S., Shieh, M.S., Pekow, P.S., Rothberg, M.B., and Hill, N.S. (2014). Outcomes associated with invasive and noninvasive ventilation among patients hospitalized with exacerbations of chronic obstructive pulmonary disease. JAMA Intern. Med. *174*, 1982–1993.
9. V A, B., Thomas, S., Philip, P.C., Thomas, A., Pillai, P., and J. P, N. (2023). Detection of Early Lung Cancer Cases in Patients with COPD Using eNose Technology: A Promising Non-Invasive Approach. In 2023 IEEE International Conference on Recent Advances in Systems Science and Engineering (RASSE), pp. 1–4.
10. V A, B., Mathew, P., Thomas, S., and Mathew, L. (2024). Detection of lung cancer and stages via breath analysis using a self-made electronicnose device. Expert Rev. Mol. Diagn. *24*, 341–353.
11. Zheng, H., Hu, Y., Dong, L., Shu, Q., Zhu, M., Li, Y., Chen, C., Gao, H., and Yang, L. (2021). Predictive diagnosis of chronic obstructive pulmonary diseaseusing serum metabolic biomarkers and least-squares supportvector machine. J. Clin. Lab. Anal. *35*.
12. Nazish, Ullah, S.I., Salam, A., Ullah, W., and Imad, M. (2021). COVID-19 Lung Image Classification Based on Logistic Regression and Support Vector Machine. In Artificial Intelligence Systems and the Internet of Things in the Digital Era, A.M. Musleh Al-Sartawi, A. Razzaque, and M.M. Kamal, eds., pp. 13–23.
13. Li, Y., Liu, Y., Guo, Y.Z., Liao, X.F., Hu, B., and Yu, T. (2022). Spatio-Temporal-Spectral Hierarchical Graph Convolutional Network With Semisupervised Active Learning for Patient-Specific Seizure Prediction. IEEE Trans. Cybern. *52*, 12189–12204.
14. Binson, V.A., Subramoniam, M., and Mathew, L. (2024). Prediction of lung cancer with a sensor array based e-nose system using machine learning methods. Microsyst. Technol. *30*, 1421–1434. https://doi.org/10.1007/s00542-024-05656-5.
15. Binson, V.A., Thomas, S., Subramoniam, M., Arun, J., Naveen, S., and Madhu, S. (2024). A Review of Machine Learning Algorithms for Biomedical Applications. Ann. Biomed. Eng. *52*, 1159–1183.
16. Cinyol, F., Baysal, U., Köksal, D., Babaoğlu, E., and Ulaşlı, S.S. (2023). Incorporating support vector machine to the classification of respiratory sounds by Convolutional Neural Network. Biomed. Signal Process Control *79*, 104093.
17. Anakal, S., and Sandhya, P. (2017). Clinical Decision Support System for Chronic Obstructive Pulmonary Disease using Machine. In International Conference on Electrical, Electronics, Communication, Computer and Optimization Techniques (ICEECCOT).
18. Mekov, E., Miravitlles, M., and Petkov, R. (2020). Artificial intelligence and machine learning in respiratory medicine. Expert Rev. Respir. Med. *14*, 559–564.
19. Zhao, S., Wang, P., Heidari, A.A., Chen, H., Turabieh, H., Mafarja, M., and Li, C. (2021). Multilevel threshold image segmentation with diffusion association slime mould algorithm and Renyi's entropy for chronic obstructive pulmonary disease. Comput. Biol. Med. *134*, 104427.
20. Zhao, D., Liu, L., Yu, F., Heidari, A.A., Wang, M., Oliva, D., Muhammad, K., and Chen, H. (2021). Ant colony optimization with horizontal and vertical crossover search: Fundamental visions for multi-threshold image segmentation. Expert Syst. Appl. *167*, 114122.
21. Dong, R., Sun, L., Ma, L., Heidari, A.A., Zhou, X., and Chen, H. (2023). Boosting Kernel Search Optimizer with Slime Mould Foraging Behavior for Combined Economic Emission Dispatch Problems. J. Bionic Eng. *20*, 2863–2895.
22. Dong, R., Liu, Y., Wang, S., Heidari, A.A., Wang, M., Chen, Y., Wang, S., Chen, H., and Zhang, Y. (2023). Multi-strategy enhanced kernel search optimization and its application in economic emission dispatch problems. J. Comput. Des. Eng. *11*, 135–172.
23. Ahmed, S., Groenli, T.-M., Lakhan, A., Chen, Y., and Liang, G. (2023). A reinforcement federated learning based strategy for urinary disease dataset processing. Comput. Biol. Med. *163*, 107210.
24. Zhou, X., Chen, Y., Gui, W., Heidari, A.A., Cai, Z., Wang, M., Chen, H., and Li, C. (2024). Enhanced differential evolution algorithm for feature selection in tuberculous pleural effusion clinical characteristics analysis. Artif. Intell. Med. *153*, 102886.
25. Wang, M., Gong, Q., Chen, H., and Gao, G. (2023). Optimizing deep transfer networks with fruit fly optimization for accurate diagnosis of diabetic retinopathy. Appl. Soft Comput. *147*, 110782.
26. Zhang, X., Wang, T., Luo, W., and Huang, P. (2021). Multi-Level Fusion and Attention-Guided CNN for Image Dehazing. IEEE Trans. Circuits Syst. Video Technol. *31*, 4162–4173.
27. Zhang, X., Wang, T., Wang, J., Tang, G., and Zhao, L. (2020). Pyramid Channel-based Feature Attention Network for image dehazing. Comput. Vis. Image Understand. *197-198*, 103003.
28. Wu, Z., Shen, S., Lian, X., Su, X., and Chen, E. (2020). A dummy-based user privacy protection approach for text information retrieval. Knowl. Base Syst. *195*, 105679.
29. Qiu, B., and Xiao, H. (2019). A Non-Stationary Geometry-Based Cooperative Scattering Channel Model for MIMO Vehicle-to-Vehicle Communication Systems. KSII Trans. Internet Inf. Syst. *13*, 2838–2858.
30. Zhang, X., Jiang, R., Wang, T., and Wang, J. (2021). Recursive Neural Network for Video Deblurring. IEEE Trans. Circuits Syst. Video Technol. *31*, 3025–3036.
31. Katoch, S., Chauhan, S.S., and Kumar, V. (2021). A review on genetic algorithm: past, present, and future. Multimed. Tools Appl. *80*, 8091–8126.
32. Yang, Y., Chen, H., Heidari, A.A., and Gandomi, A.H. (2021). Hunger games search: Visions, conception, implementation, deep analysis, perspectives, and towards performance shifts. Expert Syst. Appl. *177*, 114864.
33. Yuan, C., Zhao, D., Heidari, A.A., Liu, L., Chen, Y., Wu, Z., and Chen, H. (2024). Artemisinin optimization based on malaria therapy: Algorithm and applications to medical image segmentation. Displays *84*, 102740.
34. Yuan, C., Zhao, D., Heidari, A.A., Liu, L., Chen, Y., and Chen, H. (2024). Polar lights optimizer: Algorithm and applications in image segmentation and feature selection. Neurocomputing *607*, 128427.
35. Storn, R., and Price, K. (1997). Differential Evolution – A Simple and Efficient Heuristic for global Optimization over Continuous Spaces. J. Global Optim. *11*, 341–359.
36. Li, S., Chen, H., Wang, M., Heidari, A.A., and Mirjalili, S. (2020). Slime mould algorithm: A new method for stochastic optimization. Future Generat. Comput. Syst. *111*, 300–323.
37. Qi, A., Zhao, D., Heidari, A.A., Liu, L., Chen, Y., and Chen, H. (2024). FATA: An Efficient Optimization Method Based on Geophysics. Neurocomputing *607*, 128289.
38. Tu, J., Chen, H., Wang, M., and Gandomi, A.H. (2021). The Colony Predation Algorithm. J. Bionic Eng. *18*, 674–710.
39. Ahmadianfar, I., Heidari, A.A., Noshadian, S., Chen, H., and Gandomi, A.H. (2022). INFO: An Efficient Optimization Algorithm based on Weighted Mean of Vectors. Expert Syst. Appl. *195*, 116516.
40. Lian, J., Zhu, T., Ma, L., Wu, X., Heidari, A.A., Chen, Y., Chen, H., and Hui, G. (2024). The educational competition optimizer. Int. J. Syst. Sci. *55*, 1–38.
41. Lian, J., Hui, G., Ma, L., Zhu, T., Wu, X., Heidari, A.A., Chen, Y., and Chen, H. (2024). Parrot optimizer: Algorithm and applications to medical problems. Comput. Biol. Med. *172*, 108064.
42. Ahmadianfar, I., Heidari, A.A., Gandomi, A.H., Chu, X., and Chen, H. (2021). RUN Beyond the Metaphor: An Efficient Optimization Algorithm Based on Runge Kutta Method. Expert Syst. Appl. *181*, 115079.

43. Heidari, A.A., Mirjalili, S., Faris, H., Aljarah, I., Mafarja, M., and Chen, H. (2019). Harris hawks optimization: Algorithm and applications. Future Generat. Comput. Syst. *97*, 849–872.
44. Houssein, E.H., Oliva, D., Samee, N.A., Mahmoud, N.F., and Emam, M.M. (2023). Liver Cancer Algorithm: A novel bio-inspired optimizer. Comput. Biol. Med. *165*, 107389.
45. Chen, Z., Xuan, P., Heidari, A.A., Liu, L., Wu, C., Chen, H., Escorcia-Gutierrez, J., and Mansour, R.F. (2023). An artificial bee bare-bone hunger games search for global optimization and high-dimensional feature selection. iScience *26*, 106679.
46. Wu, S., Mao, P., Li, R., Cai, Z., Heidari, A.A., Xia, J., Chen, H., Mafarja, M., Turabieh, H., and Chen, X. (2021). Evolving fuzzy k-nearest neighbors using an enhanced sine cosine algorithm: Case study of lupus nephritis. Comput. Biol. Med. *135*, 104582.
47. Wang, M., Liang, Y., Hu, Z., Chen, S., Shi, B., Heidari, A.A., Zhang, Q., Chen, H., and Chen, X. (2022). Lupus nephritis diagnosis using enhanced moth flame algorithm with support vector machines. Comput. Biol. Med. *145*, 105435.
48. Hu, J., Han, z., Heidari, A.A., Shou, Y., Ye, H., Wang, L., Huang, X., Chen, H., Chen, Y., and Wu, P. (2022). Detection of COVID-19 severity using blood gas analysis parameters and Harris hawks optimized extreme learning machine. Comput. Biol. Med. *142*, 105166.
49. Ye, X.Y., Lyu, Z.J., and Foong, L.K. (2020). Hybridized dragonfly, whale and ant lion algorithms in enlarged pile's behavior. Smart Struct. Syst. *25*, 765–778.
50. Su, H., Zhao, D., Heidari, A.A., Liu, L., Zhang, X., Mafarja, M., and Chen, H. (2023). RIME: A physics-based optimization. Neurocomputing *532*, 183–214.
51. Garcia, S., Fernandez, A., Luengo, J., and Herrera, F. (2010). Advanced nonparametric tests for multiple comparisons in the design of experiments in computational intelligence and data mining: Experimental analysis of power. Inf. Sci. *180*, 2044–2064.
52. Derrac, J., García, S., Molina, D., and Herrera, F. (2011). A practical tutorial on the use of nonparametric statistical tests as a methodology for comparing evolutionary and swarm intelligence algorithms. Swarm Evol. Comput. *1*, 3–18.
53. Zhang, M., Wu, Q., Chen, H., Heidari, A.A., Cai, Z., Li, J., Md Abdelrahim, E., and Mansour, R.F. (2023). Whale optimization with random contraction and Rosenbrock method for COVID-19 disease prediction. Biomed. Signal Process Control *83*, 104638.
54. Zhou, W., Wang, P., Heidari, A.A., Zhao, X., and Chen, H. (2022). Spiral Gaussian mutation sine cosine algorithm: Framework and comprehensive performance optimization. Expert Syst. Appl. *209*, 118372.
55. She, Q., Hu, R., Xu, J., Liu, M., Xu, K., and Huang, H. (2022). Learning high-DOF reaching-and-grasping via dynamic representation of gripper-object interaction. Preprint at arXiv. https://doi.org/10.48550/arXiv.2204.13998.
56. Zhang, J., Liu, Y., Li, Z., and Lu, Y. (2023). Forecast-Assisted Service Function Chain Dynamic Deployment for SDN/NFV-Enabled Cloud Management Systems. IEEE Syst. J. *17*, 1–12.
57. Halaby, R., Popma, C.J., Cohen, A., Chi, G., Zacarkim, M.R., Romero, G., Goldhaber, S.Z., Hull, R., Hernandez, A., Mentz, R., et al. (2015). D-Dimer elevation and adverse outcomes. J. Thromb. Thrombolysis *39*, 55–59.
58. Thachil, J., Fitzmaurice, D.A., and Toh, C.H. (2010). Appropriate use of D-dimer in hospital patients. Am. J. Med. *123*, 17–19.
59. Galipienzo, J., Garcia de Tena, J., Flores, J., Alvarez, C., Garcia-Avello, A., and Arribas, I. (2012). Effectiveness of a diagnostic algorithm combining clinical probability, D-dimer testing, and computed tomography in patients with suspected pulmonary embolism in an emergency department. Rom. J. Intern. Med. *50*, 195–202.
60. Fu, X., Zhong, Y., Xu, W., Ju, J., Yu, M., Ge, M., Gu, X., Chen, Q., Sun, Y., Huang, H., and Shen, L. (2021). The prevalence and clinical features of pulmonary embolism in patients with AE-COPD: A meta-analysis and systematic review. PLoS One *16*, e0256480.
61. Bai, J., Liu, J., Zhang, Q., Wang, J., Fu, A., Liu, R., Zhou, X., Gao, S., and Ge, Y. (2022). A Predictive Model Based on Blood Indicators for Admission to the ICU with AECOPD. Clin. Lab. *68*.
62. Zhang, Q., Liu, J.X., Bai, J.S., Wang, J.M., Fu, A.S., Liu, R.X., Zhou, X.Y., Gao, S., Chen, Q.C., Zhang, J.B., and Ge, Y.L. (2023). D-Dimer and Procalcitonin Improve the Sensitivity of BAP-65 Score in Predicting AECOPD Patients Admission to ICU. Clin. Lab. *69*.
63. Chen, L., Xu, W., Chen, J., Zhang, H., Huang, X., Ma, L., Yu, G., Zhou, Y., Ma, B., Chen, C., et al. (2023). Evaluating the clinical role of fibrinogen, D-dimer, mean platelet volume in patients with acute exacerbation of COPD. Heart Lung *57*, 54–58.
64. Husebø, G.R., Gabazza, E.C., D'Alessandro Gabazza, C., Yasuma, T., Toda, M., Aanerud, M., Nielsen, R., Bakke, P.S., and Eagan, T.M.L. (2021). Coagulation markers as predictors for clinical events in COPD. Respirology *26*, 342–351.
65. Fruchter, O., Yigla, M., and Kramer, M.R. (2015). D-dimer as a prognostic biomarker for mortality in chronic obstructive pulmonary disease exacerbation. Am. J. Med. Sci. *349*, 29–35.
66. Hu, G., Wu, Y., Zhou, Y., Wu, Z., Wei, L., Li, Y., Peng, G., Liang, W., and Ran, P. (2016). Prognostic role of D-dimer for in-hospital and 1-year mortality in exacerbations of COPD. Int. J. Chron. Obstruct. Pulmon. Dis. *11*, 2729–2736.
67. Chang, C.C., Sorrell, T.C., and Chen, S.C.A. (2015). Pulmonary Cryptococcosis. Semin. Respir. Crit. Care Med. *36*, 681–691.
68. Lamoth, F., and Calandra, T. (2022). Pulmonary aspergillosis: diagnosis and treatment. Eur. Respir. Rev. *31*, 220114.
69. Ader, F., Nseir, S., Le Berre, R., Leroy, S., Tillie-Leblond, I., Marquette, C.H., and Durocher, A. (2005). Invasive pulmonary aspergillosis in chronic obstructive pulmonary disease: an emerging fungal pathogen. Clin. Microbiol. Infect. *11*, 427–429.
70. Bafadhel, M., McKenna, S., Agbetile, J., Fairs, A., Desai, D., Mistry, V., Morley, J.P., Pancholi, M., Pavord, I.D., Wardlaw, A.J., et al. (2014). Aspergillus fumigatus during stable state and exacerbations of COPD. Eur. Respir. J. *43*, 64–71.
71. Mir, T., Uddin, M., Khalil, A., Lohia, P., Porter, L., Regmi, N., Weinberger, J., Koul, P.A., and Soubani, A.O. (2022). Mortality outcomes associated with invasive aspergillosis among acute exacerbation of chronic obstructive pulmonary disease patient population. Respir. Med. *191*, 106720.
72. Barberán, J., García-Pérez, F.J., Villena, V., Fernández-Villar, A., Malmierca, E., Salas, C., Giménez, M.J., Granizo, J.J., and Aguilar, L. (2017). Development of Aspergillosis in a cohort of non-neutropenic, non-transplant patients colonised by Aspergillus spp. BMC Infect. Dis. *17*, 34.
73. Leung, J.M., Tiew, P.Y., Mac Aogáin, M., Budden, K.F., Yong, V.F.L., Thomas, S.S., Pethe, K., Hansbro, P.M., and Chotirmall, S.H. (2017). The role of acute and chronic respiratory colonization and infections in the pathogenesis of COPD. Respirology *22*, 634–650.
74. Morris, A., Alexander, T., Radhi, S., Lucht, L., Sciurba, F.C., Kolls, J.K., Srivastava, R., Steele, C., and Norris, K.A. (2009). Airway obstruction is increased in pneumocystis-colonized human immunodeficiency virus-infected outpatients. J. Clin. Microbiol. *47*, 3773–3776.
75. Domenech, A., Puig, C., Martí, S., Santos, S., Fernández, A., Calatayud, L., Dorca, J., Ardanuy, C., and Liñares, J. (2013). Infectious etiology of acute exacerbations in severe COPD patients. J. Infect. *67*, 516–523.
76. de Miguel Díez, J., Chancafe Morgan, J., and Jiménez García, R. (2013). The association between COPD and heart failure risk: a review. Int. J. Chron. Obstruct. Pulmon. Dis. *8*, 305–312.
77. Marcun, R., Sustic, A., Brguljan, P.M., Kadivec, S., Farkas, J., Kosnik, M., Coats, A.J.S., Anker, S.D., and Lainscak, M. (2012). Cardiac biomarkers predict outcome after hospitalisation for an acute exacerbation of chronic obstructive pulmonary disease. Int. J. Cardiol. *161*, 156–159.
78. Chang, C.L., Robinson, S.C., Mills, G.D., Sullivan, G.D., Karalus, N.C., McLachlan, J.D., and Hancox, R.J. (2011). Biochemical markers of cardiac dysfunction predict mortality in acute exacerbations of COPD. Thorax *66*, 764–768.
79. Tinè, M., Bazzan, E., Semenzato, U., Biondini, D., Cocconcelli, E., Balestro, E., Casara, A., Baraldo, S., Turato, G., Cosio, M.G., and Saetta, M. (2020). Heart Failure is Highly Prevalent and Difficult to Diagnose in Severe Exacerbations of COPD Presenting to the Emergency Department. J. Clin. Med. *9*.
80. Peng, L.G., Zhou, C., Zhou, H.X., Luo, Y.M., Ge, H.Q., Liu, H.G., Wei, H.L., Zhang, J.C., Pan, P.H., Zhang, J.R., et al. (2021). Risk factors associated with in-hospital mortality in hospitalized patients with acute exacerbation of chronic obstructive pulmonary disease: a multicenter retrospective study. Zhonghua Yixue Zazhi *101*, 3932–3937.
81. Curkendall, S.M., DeLuise, C., Jones, J.K., Lanes, S., Stang, M.R., Goehring, E., Jr., and She, D. (2006). Cardiovascular disease in patients with chronic obstructive pulmonary disease, Saskatchewan Canada cardiovascular disease in COPD patients. Ann. Epidemiol. *16*, 63–70.
82. Cao, Y., Xing, Z., Long, H., Huang, Y., Zeng, P., Janssens, J.P., and Guo, Y. (2021). Predictors of mortality in COPD exacerbation cases presenting to the respiratory intensive care unit. Respir. Res. *22*, 77.
83. Cruz-Jentoft, A.J., Bahat, G., Bauer, J., Boirie, Y., Bruyère, O., Cederholm, T., Cooper, C., Landi, F., Rolland, Y., Sayer, A.A., et al. (2019). Sarcopenia: revised European consensus on definition and diagnosis. Age Ageing *48*, 601.
84. Benz, E., Trajanoska, K., Lahousse, L., Schoufour, J.D., Terzikhan, N., De Roos, E., de Jonge, G.B., Williams, R., Franco, O.H., Brusselle, G., and Rivadeneira, F. (2019). Sarcopenia in COPD: a systematic review and meta-analysis. Eur. Respir. Rev. *28*, 190049.
85. Tanimura, K., Sato, S., Fuseya, Y., Hasegawa, K., Uemasu, K., Sato, A., Oguma, T., Hirai, T., Mishima, M., and Muro, S. (2016).

Quantitative Assessment of Erector Spinae Muscles in Patients with Chronic Obstructive Pulmonary Disease. Novel Chest Computed Tomography-derived Index for Prognosis. Ann. Am. Thorac. Soc. *13*, 334–341.

86. McDonald, M.L.N., Diaz, A.A., Ross, J.C., San Jose Estepar, R., Zhou, L., Regan, E.A., Eckbo, E., Muralidhar, N., Come, C.E., Cho, M.H., et al. (2014). Quantitative computed tomography measures of pectoralis muscle area and disease severity in chronic obstructive pulmonary disease. A cross-sectional study. Ann. Am. Thorac. Soc. *11*, 326–334.
87. Mason, S.E., Moreta-Martinez, R., Labaki, W.W., Strand, M., Baraghoshi, D., Regan, E.A., Bon, J., San Jose Estepar, R., Casaburi, R., McDonald, M.L.N., et al. (2021). Respiratory exacerbations are associated with muscle loss in current and former smokers. Thorax *76*, 554–560.
88. Wilson, A.C., Bon, J.M., Mason, S., Diaz, A.A., Lutz, S.M., Estepar, R.S.J., Kinney, G.L., Hokanson, J.E., Rennard, S.I., Casaburi, R., et al. (2022). Increased chest CT derived bone and muscle measures capture markers of improved morbidity and mortality in COPD. Respir. Res. *23*, 311.
89. Jadhav, S., He, H., and Jenkins, K. (2018). Information gain directed genetic algorithm wrapper feature selection for credit rating. Appl. Soft Comput. *69*, 541–553.
90. Tempola, F., Rosihan, R., and Adawiyah, R. (2021). Holdout Validation for Comparison Classfication Naïve Bayes and KNN of Recipient Kartu Indonesia Pintar. IOP Conf. Ser. Mater. Sci. Eng. *1125*, 012041.
91. HoKun, J., and ChanSu, Y. (2021). Enhancement of Ship Type Classification from a Combination of CNN and KNN. Electronics *10*, 1169.
92. Fan, Z., Xie, J.K., Wang, Z.Y., Liu, P.C., Qu, S.J., and Huo, L. (2021). Image Classification Method Based on Improved KNN Algorithm. J. Phys. Conf. *1930*, 012009.
93. Tu, Q., Chen, X., and Liu, X. (2019). Multi-strategy ensemble grey wolf optimizer and its application to feature selection. Appl. Soft Comput. *76*, 16–30.
94. Storn, R., and Price, K. (1996). Minimizing the real functions of the ICEC'96 contest by differential evolution. In Proceedings of IEEE International Conference on Evolutionary Computation, pp. 842–844.
95. Emary, E., Zawbaa, H.M., and Hassanien, A.E. (2016). Binary grey wolf optimization approaches for feature selection. Neurocomputing *172*, 371–381.

STAR★METHODS

KEY RESOURCES TABLE

REAGENT or RESOURCE	SOURCE	IDENTIFIER
Software and algorithms		
RIME algorithm	Ali Asghar Heidari	https://aliasgharheidari.com/RIME.html
DDRIME algorithm	This paper	DDRIME (zenodo.org)

METHOD DETAILS

The proposed approach consists of RIME optimization, KNN model, dispersed foraging strategy, differential crossover operator, explained in detail in this section.

RIME optimization

RIME[50] proposed in 2023, is an innovative MA inspired by the formation of rime ice. The algorithm consists of four steps: (1) initializing the rime cluster; (2) using a soft-rime search method to explore by imitating the movement of soft-rime agents; (3) applying a hard-rime puncture strategy to exploit by replicating the crossover behavior among hard-rime individuals; (4) implementing a positive greedy selection strategy. The mathematical formulation is detailed below.

The initializing of Rime clusters

Similar to various other MAs, RIME treats each rime as a search agent and initializes N search agents randomly within the search space to form a new population X. The initialization process of population X is shown as Equation 7.

$$X = \begin{bmatrix} x_{11} & x_{12} & \cdots & x_{1D} \\ x_{21} & x_{22} & \cdots & x_{2D} \\ \vdots & \vdots & \ddots & \vdots \\ x_{N1} & x_{N2} & \cdots & x_{ND} \end{bmatrix} \quad \text{(Equation 7)}$$

$$X_i^j = LB_i^j + \text{rand} \times \left(UB_i^j - LB_i^j\right); i \in \{1,2,\ldots,N\}, j \in \{1,2,\ldots,D\} \quad \text{(Equation 8)}$$

where D is the problem dimension. i is the index of the rime particle and j denotes the dimension of the rime agent. *rand* signifies a random value in the range [0,1]. *UB* and *LB* are the maximum and minimum limits of the search space.

Soft-rime search

The inherent randomness of the soft-rime growth process enables it to adhere to most surfaces of an object, although soft-rime grows slowly when moving in the same direction. Consequently, the soft-rime search strategy leverages these growth characteristics, enabling RIME to explore a broad search space during the initial iterations and prevent local stagnation effectively. The rime-particles update procedure is as Equation 9.

$$X_{new_i}^j = X_{best}^j + r_1 \cdot \cos\theta \cdot \beta \cdot \left(h \cdot \left(UB_i^j - LB_i^j\right) + LB_i^j\right), r_2 < E \quad \text{(Equation 9)}$$

where $X_{new_i}^j$ denotes the j^{th} particle of the i^{th} rime-agent's newly updated position. X_{best}^j stands for the j^{th} particle of the current population's best-rime individual. r_1 denotes a control parameter for the particle movement direction, randomly set within the range [-1,1]. cos θ fluctuates with the iterations and can be computed by Equation 10.

$$\theta = \pi \cdot (g / 10 \cdot G) \quad \text{(Equation 10)}$$

where G denotes the maximum number of evaluations, g represents the current evaluation. β is an environmental factor that adjusts with the number of iterations, reflecting external influences to facilitate convergence. The mathematical expression is given as Equation 11.

$$\beta = 1 - \left[\frac{w \cdot g}{G}\right] \Big/ w \quad \text{(Equation 11)}$$

where [.] is rounding, and w equals 5. Consequently, the value of β is determined by a step function. E represents an adhesion factor that affects the condensation probability, as illustrated in Equation 12.

$$E = \sqrt{(g/G)} \quad \text{(Equation 12)}$$

Hard-rime search

Hard rime grows in the same direction, allowing rime agents to intersect easily—a phenomenon known as rime puncture. Drawing inspiration from this, we propose the hard-rime puncture strategy to facilitate exchanges between search agents within the rime population. This mechanism enhances RIME's convergence and effectively prevents it from settling into local optima. It can be formulated as Equation 13.

$$X_{new_i}^{j} = X_{best}^{j}, r_3 < F^{normr}(X_i) \quad \text{(Equation 13)}$$

where $F^{normr}(X_i)$ means the normalized value of the i^{th} search agent's fitness value, which shows the probability of this agent being selected. r_3 denotes a number randomly generated within the range of -1 to 1.

Positive greedy selection

To address the limited contribution of the conventional greedy selection mechanism to further exploration and exploitation during population updates, RIME introduces a positive greedy selection mechanism. This enhanced approach compares the fitness of updated search agents with their non-updated counterparts. If the updated fitness is better, the non-updated agent and its fitness value are replaced, concurrently updating the best search agent. The method elevates the quality of search agents, steering the population towards a more favorable evolution with every iteration. The source code for this mechanism is detailed in Algorithm 1. The flowchart of RIME is presented in Figure S1.

Algorithm 1. RIME

Initialize the rime population $X_i(i = 1,2,\ldots,N)$;
  Define the fitness $F(X_i)$ of X_i;
  Get the best rime-agent X_{best} and corresponding fitness value $F(X_{best})$;
  While ($g \leq G$)
    Calculate the factor of being adherence E by Equation 12;
    For i =1: N
    For j =1: D
    // soft-rime search strategy
    If $r_2 < E$
    Calculate the position of $X_{new_i}^{j}$ by Equation 9;
    End
    // hard-rime search strategy
    If $r_3 < F^{normr}(X_i)$
    Calculate the position of $X_{new_i}^{j}$ by Equation 13;
    End
    End
    Update the fitness value $F(X_{new\,i})$ of $X_{new\,i}$;
    // greedy selection mechanism
    If $F(X_{new\,i}) < F(X_i)$
    $F(X_i) = F(X_{new\,i})$;
    $X_i = X_{new\,i}$;
    If $F(X_{new\,i}) < F(X_{best})$
    $F(X_{best}) = F(X_{new\,i})$;
    $X_{best} = X_{new\,i}$;
    End
    End
    End
    $g = g+1$;
  End
  Return $X_{best}, F(X_{best})$;

KNN model

K-nearest neighbor (KNN) [89] is a kind of classification algorithm, which represents a non-parametric methodology. It shows exceptional performance in approximate tasks, presenting high success rates and accurate classification.[90–92] Its core idea is to determine the category of samples by calculating the distance between them. In the KNN algorithm, K represents the selection of K nearest neighbors whose categories are used to classify unknown samples. If most of the near neighbors belong to a class, the unknown sample is assigned to that class. The KNN

classifier has many advantages. First, it is simple to implement and understand. Secondly, the KNN algorithm is suitable for a variety of different types of data, including continuous data and discrete data. In addition, the KNN algorithm can effectively deal with multiple classification problems and can deal with difficult to separate problems. It classifies a new instance by taking a majority vote from KNN models. The class is identified by determining the minimum distance to a training point, typically using a similarity measure such as Euclidean distance, as outlined in the literature. Mathematical expression to calculate the Euclidean distance between Z_1 and Z_2 which represent two points in the D-dimensional space shown Equation 14.

$$Distance\,(Z_1, Z_2) = \left(\sum_{i=1}^{D} \left(z_1^i - z_2^i\right)^2\right)^{\frac{1}{2}} \quad \text{(Equation 14)}$$

In this research, the KNN classifier is used to evaluate its training speed, easy implementation and remarkable classification accuracy.

The dispersed foraging strategy

Although Su et al. identified the limitations and opportunities for improvement, RIME still has substantial room for further development to reduce the likelihood of being affected by local minima. In times of food scarcity, a dispersed foraging mechanism drives part of the population to explore new areas in search of sustenance. It allows them to locate their prey. A new method of foraging involving dispersion is put forward to construct a mathematical formula for this behavior.[93] During scattered foraging, search individuals update their positions as Equation 15.

$$X(t+1) = X(t) + \rho \cdot (X_m(t) - X_n(t)) \quad \text{(Equation 15)}$$

where $t+1$ is the next iteration number and t denotes the current iteration; X (t + 1) denotes the updated position and X (t) represents the current position. Assume that the scale control factor $\rho \sim N(0.5, 0.12)$ is distributed according to $N(0.5, 0.12)$ distribution, where the two integers m and n are greater than 1 and less than N, independently. As shown in Equation 16, a new adaptive parameter named dispersal rate (DR) is introduced. DR determines which agent seeks out the new food source. The result parameter r for comparison with DR is added to get this control. To speed up convergence, when $r > DR$, an individual is classified as a forager; when $r < DR$, an individual is taken as an ordinary individual. In additional, with a gradual increase in the number of examinations, DR will decline over time.

As the hungry agents approach the optimal value, they risk falling into a local optimum if they are not dispersed at this stage. At the same time, with the increase of evaluation times, DR gradually decreases, ensuring that the latest method will not fall into the local optima.

$$DR = DR_{max} - (DR_{max} - DR_{min}) \cdot \frac{t}{Max_{iter}} \quad \text{(Equation 16)}$$

$$X(t+1) = \begin{cases} X(t) + \rho \cdot (X_m(t) - X_n(t)), \, if \; r > DR \\ X(t), \, otherwise \end{cases} \quad \text{(Equation 17)}$$

where Max_{iter} represents the upper limit of iterations. r shows the number randomly generated between 0 and 1, the parameter ρ encourages individuals to exhibit more randomness in their actions. The adaptive parameter DR regulates the size of individuals dispersed into the new domain. The search agent is repositioned in a decentralized process at the beginning of iteration with a large DR, which contributes to a faster convergence rate. As the DR decreases with more iterations, individuals are more likely to become discrete, helping the algorithm avoid local optimality. Algorithm 2 presents the pseudo-code of the dispersed foraging mechanism.

Algorithm 2. Dispersed foraging

Input: The parameter DR, search population $X(t)$

Output: The search individual population $X(t+1)$

Calculate the dispersed distance parameter DR using Equation 16

Compute the position of search individual $X(t)$ using Equation 17

The differential crossover operator

R. Storn and K. Price proposed differential evolution (DE) which is a probabilistic and reliable metaheuristic optimizer.[94] Due to the various advantages of GA, different fields usually integrate the characteristics of quick convergence, simple structure, and high robustness into their systems. Four basic steps of DE are the initializing of the population, the mutation, the crossover, and the selection. Among these, the mutation and crossover operators are important to the effective of their optimization process. The mutation of DE is expressed as Equation 18.

$$V_i(t) = X_{r1}(t) + beta \times (X_{r2}(t) - X_{r3}(t)) \quad \text{(Equation 18)}$$

where $r1, r2,$ and $r3$ are three random integers mutually exclusive in the generated interval 1 *to N, beta* represents the scale parameter. Then, the new position $X(t+1)$ updates according to Equation 19.

$$X_{i,j}(t+1) = \begin{cases} V_{i,j}(t) & if\ (rand \leq CR\ or\ j = j_{rand}) \\ X_{i,j}(t) & otherwise \end{cases} \quad \text{(Equation 19)}$$

CR is the crossover factor to find the better agent, which influences the genetic information of the parents. $j \in \{1, 2, \ldots\ldots, D\}$ where j_{rand} represents an integer between 1 and D, where D denotes the individuals' dimensions. $V_i(t)$ denotes the crossed individual. There is Algorithm 3 that shows the code of the differential crossover operator.

Algorithm 3. Pseudo-code of differential crossover operator

Input: Hungry search population $X(t)$, parameter CR;
Output: The hungry search population $X(t+1)$;
for $i = 1$ *to* N **do**
carry out the DE mutation operation by Equation 18;
for $j = 1$ *to* D **do**
Calculate the position of the hungry search individual $X_{i,j}(t+1)$ by Equation 19;
End
End

Proposed methodology

DDRIME algorithm for global optimization

In the work, we initiate the process by updating the population by an interactive mechanism. Selecting two agents from the population randomly and enabling information exchange with the current population, we help them acquire more data and improve their expressive capabilities. Following this, we apply the RIME algorithm steps to further develop the individuals, using a dispersed foraging mechanism to select the optimal positions. Thus, we boost the exploration of the search space by utilizing a differential crossover operator, thereby raising the chances of discovering the optimal solution. The work chart of DDRIME is presented in Figure S2.

Binary DDRIME for feature selection

DDRIME is an enhanced continuous version of the RIME algorithm, its discrete binary version can obtain useful feature information. Dispersed foraging mechanism and differential crossover operator help RIME select crucial features, generate the most suitable scheme and improve classification accuracy. Given that feature selection is a binary problem, the solution is restricted to the binary space.[1] In summary, DDRIME should adopt a binary format for feature selection. An n-dimensional vector represents the length that is the total number of metrics in the dataset. Besides, the value of the solution is "0" or "1", where "0" indicates that the feature is not chosen and "1" signifies that the feature is selected as crucial. The individual initialization and binary position vectors are expressed by Equation 20 using a random threshold.

$$X_i^j = \begin{cases} 0 & rand \leq 0.5 \\ 1 & rand > 0.5 \end{cases} \quad \text{(Equation 20)}$$

where X_i^j is the *ith* individual of the population vector in the *jth* dimension. Then, DDRIME converts to binary DDRIME (bDDRIME) by a transfer function (TF). The updating strategy of TF in the research is shown in Equation 21.

$$T\left(X_i^j(t)\right) = \left|\frac{2}{\pi}\arctan\left(\frac{\sqrt{\pi}}{2}X_i^j(t)\right)\right| \quad \text{(Equation 21)}$$

where $X_i^j(t)$ is the *i*th agent in *jth* dimension at *t*th iteration and $X_i^j(t+1)$ denotes its next iteration calculated by Equation 22.

$$X_i^j(t+1) = \begin{cases} -X_i^j(t+1), & rand < T\left(x_i^d(t+1)\right) \\ X_i^j(t+1), & rand \geq T\left(x_i^d(t+1)\right) \end{cases} \quad \text{(Equation 22)}$$

Two indicators for feature selection are classification accuracy and the number of features selected. An improved classification result is characterized by higher accuracy with a smaller number of selected features. Besides, a fitness function assesses each solution's quality across the iteration. Thus, bDDRIME keeps the balance between two indicators and the expression of the fitness function is shown as Equation 23.

$$Fitness = \alpha \cdot (1 - Acc) + (1 - \alpha) \times (D_R / D) \quad \text{(Equation 23)}$$

where α is the weight factor and $\alpha = 0.05$[95] is selected from relevant literature; Acc represents classification accuracy; D_R shows the size of the optimized subset, and D represents the total number of features in the dataset.

Scale the range of the dataset to [-1,1] and divide the dataset into a training set and a test set. Ten-fold cross-validation is employed in this study. The binary DDRIME population is initialized, with the dimension of bDDRIME corresponding to the number of attributes in the dataset. We then adopt the KNN classifier to build the bDDRIME-KNN model which calculates the population's fitness and solves the optimal solution. Therefore, the optimal feature subset is outputted by the bDDRIME-KNN model. There is this model's flowchart in Figure S3.

QUANTIFICATION AND STATISTICAL ANALYSIS

A comprehensive explanation of the statistical techniques employed can be found in the "results and discussion" section, which includes the following parts: "Verification of the Mechanisms," "Comparison with Standard Metaheuristic Algorithms," "Comparison with Several Enhanced Algorithms," and "Feature Selection." Its noteworthy that all the experiments were performed consistently using the same hardware setup and the MATLAB R2018b platform. In this research, the statistical analysis is conducted using SPSS version 26.0. For continuous variables that are normally distributed, the Kolmogorov-Smirnov test was applied, and the results are expressed as the mean plus or minus the standard deviation (mean $\pm$ SD). The u test is then used for comparative analysis. For continuous variables that do not follow a normal distribution, non-parametric tests are employed, and the data is depicted as the median with the interquartile range (IQR). Categorical data are displayed as percentages, and group comparisons are made using either the chi-square test or Fisher's exact test when appropriate. Table 1 enumerates all the variables measured, while the statistical analyses for these variables are detailed in Tables 2 and 3.

In terms of global optimization problem, these methods including DDRIME algorithm evaluated their performance using the statistical average value of the optimal function (AVG) and standard deviation (STD). The smaller the value, the better the performance. If the modification is considered significant statistically, the Wilcoxon signed-rank test is less than 0.05; that is, the p-value is less than 0.05. The Wilcoxon signed-rank test is a non-parametric statistical test at a significance level of 0.05. The Friedman test is a statistical conformance test, too. The symbols "+/=/-" illustrate that the proposed algorithm performs better, equal, or worse than the other comparative method. All statistical details of global optimization are provided in Tables 5, 6, and 7 and Figure 1. The results are evaluated in terms of classification accuracy, number of selected features, and mean and standard deviation of fitness and run time as Figures 4 and 5. Tables 8, 9, 10, and 11 and Figure 3 describe the statistical outcomes of the 12 high-dimensional gene datasets simulated by intelligent swarm algorithms. All statistical details are provided and explained in the text.